The Simplified Ionospheric Regional Model (SIRM) for HF Prediction: Basic Theory, Its Evolution and Applications

M. Pietrella, M. Pezzopane, B. Zolesi, Lj. R. Cander & A. Pignalberi

Surveys in Geophysics
An International Review Journal
Covering the Entire Field of Earth and Space Sciences

ISSN 0169-3298

Surv Geophys
DOI 10.1007/s10712-020-09600-w

Springer

Surveys in Geophysics
https://doi.org/10.1007/s10712-020-09600-w

The Simplified Ionospheric Regional Model (SIRM) for HF Prediction: Basic Theory, Its Evolution and Applications

M. Pietrella[1] · M. Pezzopane[1] · B. Zolesi[1] · Lj. R. Cander[2] · A. Pignalberi[1]

Received: 20 February 2020 / Accepted: 25 June 2020

Abstract
This paper is a final review of the Simplified Ionospheric Regional Model (SIRM) developed as a prototype in the early 1990s and improved in the following years. By means of an algorithm based on the Fourier synthesis, the SIRM model in its prototype version provides predicted monthly median values of the main ionospheric characteristics such as: the ordinary wave critical frequencies (*fo*E, *fo*F1, and *fo*F2) of the E, F1, and F2 ionospheric layers; the lowest virtual height (*h*'F) of the ordinary trace of the F region; the obliquity factor for a distance of 3000 km (*M*(3000)F2). Instead, the improved version focuses only on *fo*F2 and *M*(3000)F2. The SIRM model has been largely employed in the framework of different international research projects as the climatological reference to output *fo*F2 and *M*(3000)F2 monthly median predictions, but in its SIRMUP version is used also as a nowcasting model and as an intermediate step of complex procedures for a near real-time three-dimensional representation of the ionospheric electron density. In this regard, some results provided by both SIRM and SIRMUP for telecommunication applications are shown. Moreover, the mathematical treatment concerning both the phase correction of the Fourier synthesis and the fundamental steps carried out to define the SIRM algorithm in its final version, never published so far, will be described in detail in dedicated Appendices. Finally, for the first time the SIRM code is now downloadable for the benefit of users.

Keywords SIRM · SIRMUP · *fo*F2 · *M*(3000)F2 · Regional modelling

1 Introduction

In recent decades, ionosonde systems able to autoscale ionograms (Reinisch and Huang 1983; Reinisch et al. 2005; Galkin and Reinisch 2008; Stankov et al. 2012; Pezzopane and Scotto 2005, 2007; Scotto and Pezzopane 2002; Scotto 2009) have allowed the development of ionospheric nowcasting tools. These, by ingesting in near real-time the two most important ionospheric characteristics for high-frequency (HF) radio propagation purposes, i.e. the ionospheric F2 region ordinary critical frequency (*fo*F2) and the obliquity

✉ A. Pignalberi
alessio.pignalberi@ingv.it

[1] Istituto Nazionale di Geofisica e Vulcanologia, Via di Vigna Murata 605, 00143 Rome, Italy

[2] Rutherford Appleton Laboratory, Harwell Oxford, Oxon OX11 0QX, UK

Published online: 18 July 2020

factor for a distance of 3000 km (M(3000)F2), provide a near real-time picture of the ionosphere on a local, regional, and global scale.

Nowcasting models (Zolesi et al. 2004; Tsagouri et al. 2005; Pietrella and Perrone 2005; Pietrella 2015; Pezzopane et al. 2011, 2013; Pietrella et al. 2018; Pignalberi et al. 2018a, b) represent valuable tools in a space weather context. They became very useful to plan a reliable HF sky-wave telecommunication system under disturbed geomagnetic conditions in general, and during ionospheric storm events in particular. For instance, consulting foF2 and M(3000)F2 nowcasting maps, HF operators can get important indications about the Maximum Usable Frequencies (MUFs) for a point-to-point radio link (Zolesi and Cander 2014).

Likewise, forecasting models are important (Cander et al. 1998; Muhtarov and Kutiev 1999; Stanislawska and Zbyszynski 2002; Oyeyemi et al. 2005; Strangeways et al. 2009; Pietrella 2012; Mikhailov and Perrone 2014). Indeed, they play an important role in replacing nowcasting procedures when autoscaled data are unavailable. The data unavailability can be due to either ionosonde malfunctions or a highly disturbed ionosphere triggered by severe space weather conditions (Cander 2019).

In the past, when nowcasting and forecasting models were still under development, ionospheric modelling for both research and application relied on global climatological models that provided long-term predictions of the monthly median values of the main ionospheric characteristics. Jones and Gallet (1962, 1965) developed a numerical mapping procedure to generate CCIR (International Radio Consultative Committee) global maps of foF2 and M(3000)F2 monthly median values for high and low solar activity, suggesting a linear interpolation of the underlying temporal and spatial expansions coefficients for intermediate levels of solar activity. A well-known climatological global model is NeQuick2 (Nava et al. 2008 and references therein), the second version of the NeQuick model (Hochegger et al. 2000; Radicella and Leitinger 2001). Nevertheless, over the years, the International Reference Ionosphere (IRI) model has been, and it is still today, the reference climatological global model for the ionospheric community (Bilitza 1986, 1995, 1997, 2001, 2018; Bilitza and Reinisch 2008; Bilitza et al. 1990, 2014). In April 2014, IRI became the official International Standardization Organization (ISO) standard for the ionosphere (Bilitza et al. 2017).

Several regional models were also proposed (e.g., Dvinskikh 1988; Singer and Dvinskikh 1991; Zolesi et al. 1993; Reinisch et al. 1993; Mikhailov et al. 1996; De Franceschi and De Santis 1994; Bradley et al. 1994; Hanbaba 1999; Karpachev et al. 2016, 2018; Karpachev 2019; Themens et al. 2017, 2018, 2019), because they can "capture" the ionospheric variability in a relatively small area better than global models, thus providing more reliable predictions. Among these, a prototype of the Simplified Ionospheric Regional Model (SIRM) was developed in the early 1990s with the aim to improve the accuracy of the monthly median predictions of the main ionospheric characteristics provided by the pre-existing global models (Zolesi et al. 1993, 1994).

The SIRM prototype was developed analysing the historical database coming from seven reference ionospheric stations located inside a restricted sector of the European region. It predicts the monthly median values of the main ionospheric characteristics, i.e. the ordinary critical frequency foE and foF1 of E and F1 ionospheric regions, foF2, the lowest virtual height h'F of the ordinary trace of the F region, and M(3000)F2. The predictions were produced on a yearly base through the Fourier synthesis using only 100 numerical coefficients.

The SIRM prototype was later re-evaluated making some changes aimed at further improving the accuracy of foF2 and M(3000)F2 predictions. The most important

modifications consisted in: (a) considering a greater number of reference historical databases; (b) correcting the phase Fourier coefficients; (c) considering a different solar activity index. Based on the new added datasets from more ionospheric stations, collected during the COST (Cooperation in the field of Scientific and Technical Research) Action 251 on "Improved quality of services in Ionospheric Telecommunication Systems planning and operation" (Hanbaba 1999), Fourier coefficients were recalculated. This has allowed to generation of *fo*F2 and *M*(3000)F2 time series by means of the Fourier synthesis using 100 numerical coefficients per month so that the whole model, differently from the SIRM prototype, is represented by a total of $100 \times 12 = 1200$ Fourier coefficients in the follow up improved version of the SIRM model.

Although the SIRM model was born as a long-term prediction model, by using an effective solar activity index (Houminer et al. 1993) calculated on the basis of *fo*F2 and *M*(3000)F2 autoscaled data at defined reference ionospheric stations, it can be updated and then employed as a nowcasting model in its validity area. This gave rise to the development of the SIRM UPdated (SIRMUP) version of the improved SIRM (Zolesi et al. 2004). The SIRM model, and its SIRMUP version, have been largely used in recent decades in the framework of several international research projects (Tsagouri et al. 2005, 2013; Belehaki et al. 2007, 2015; Pietrella 2015). It has been also used as an intermediate step of operational nowcasting applications, for a near real-time three-dimensional representation of the ionospheric electron density (Pezzopane et al. 2011, 2013; Pietrella et al. 2018). Despite of all this, neither its formulation has ever been fully published in a scientific journal nor its Fortran code has ever been shared. Here is the reason for this revision that is also accompanied by two Appendices where the novelties about the SIRM in its improved version are described in detail, and by a link through which the reader will be able to download the SIRM Fortran code.

The SIRM prototype will be described in Sect. 2, where some preliminary considerations useful for describing its improved version will be also given. Section 3 focuses on the evolution of SIRM prototype and its applications over the past years in the context of some international projects. The SIRMUP model and its applications are the subject of Sect. 4, while concluding remarks and possible future developments about the SIRM approach are respectively summarized and outlined in Sect. 5. Moreover: Appendix 1.1 shows the mathematical apparatus concerning the phase correction of the Fourier synthesis; Appendix 1.2 reports the main steps which are behind the formulation of the improved SIRM algorithm.

2 The SIRM Prototype

2.1 Database and Validity Area

The SIRM prototype was developed in the early 1990s, in the framework of the COST Action 238 on "Prediction and Retrospective Ionospheric Modelling over Europe (PRIME)" (Bradley 1995). It should be pointed out that the first version of the SIRM model has never been applied in any research project, but only some tests were carried out to investigate its performance. For this reason, we refer to it as the SIRM prototype. Anyhow, such tests have been useful to encourage further improvements.

The Centre National d'Etudes des Telecommunications (CNET) in Lannion (France) and the World data Center-A in Boulder (Colorado, USA) are the institutions that provided the dataset used to develop the SIRM prototype. This dataset is formed by the

Table 1 Geographic longitude and latitude and available dataset of the seven ionospheric stations used to develop the SIRM prototype

Station	Geographic longitude	Geographic latitude	Years of available data
Gibilmanna	14.0° E	37.6° E	1976–1979 and 1984–1987
Rome	12.5° E	41.9° N	1957–1987
Belgrade/Grocka	20.5° E	44.8° N	1964–1985
Poitiers	0.3° E	46.6° N	1964–1984
Lannion	3.4° W	48.7° N	1971–1984
De Bilt	5.2° E	52.1° N	1968–1976
Uppsala	17.6° E	59.8° N	1967–1976

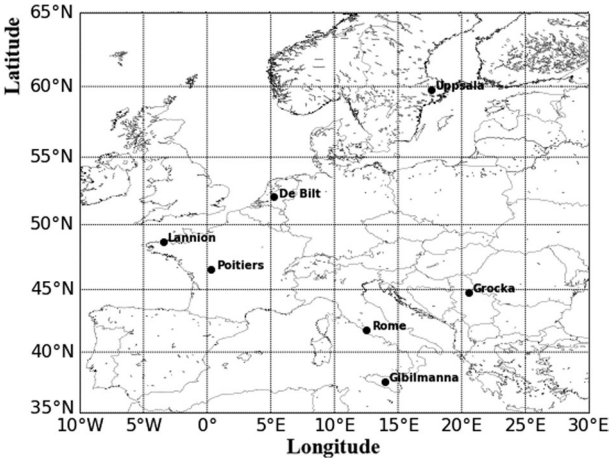

Fig. 1 Position of the seven ionospheric stations used as reference to develop the SIRM prototype

hourly monthly median values of *fo*E, *fo*F1, *fo*F2, *h*'F, and *M*(3000)F2 manually validated, recorded in seven reference ionospheric stations positioned in the region extending in longitude from 3.5° W to 20.5° E and in latitude from 38° N to 60° N. Table 1 gives information about these seven stations, while Fig. 1 shows their position within the European area.

2.2 Model Formulation

The development of the SIRM prototype consisted of six main steps:

1. Achievement of empirical prediction models for the ionospheric stations listed in Table 1, by means of a linear regression analysis between the monthly median values of the ionospheric characteristic (generally indicated as Ω) taken at the local standard time (LT), against the monthly mean solar sunspot number R. Specifically, at a definite station ($s = 1,\ldots,7$), the ionospheric characteristic can be predicted at a given hour (h) and month (m) by using the linear prediction algorithm

$$\Omega(h,m,R)_s = \alpha(h,m)_s R + \beta(h,m)_s, \tag{1}$$

where $\alpha(h,m)_s$ and $\beta(h,m)_s$ are the coefficients calculated at the station s, known by the regression analysis carried out between the monthly median values (collected at the hour h and month m) and corresponding R. Therefore, the formula

$$\Omega(R)_s = \sum_{m=1}^{12}\sum_{h=1}^{24}\Omega(h,m,R)_s = \sum_{m=1}^{12}\sum_{h=1}^{24}\left(\alpha(h,m)_s R + \beta(h,m)_s\right) \tag{2}$$

provides for a given value of R the yearly time series predictions of any ionospheric characteristic in each of the seven considered reference ionospheric stations.

2. Achievement for each reference station of two time series: one for $R=0$ identified as $\Omega(R=0)_s$ and the other one for $R=100$ identified as $\Omega(R=100)_s$. These time series are defined with the aim to linearly interpolate between them to get the best prediction of the ionospheric characteristic for a generic value of R.
3. Fourier synthesis of $\Omega(R=0)_s$ and $\Omega(R=100)_s$ as:

$$\Omega(t,R=0)_s = A(R=0)_{s,0} + \sum_{n=1}^{144} A(R=0)_{s,n}\sin\left(\frac{2\pi nt}{T} + Y(R=0)_{s,n}\right), \tag{3a}$$

$$\Omega(t,R=100)_s = A(R=100)_{s,0} + \sum_{n=1}^{144} A(R=100)_{s,n}\sin\left(\frac{2\pi nt}{T} + Y(R=100)_{s,n}\right); \tag{3b}$$

$A(R=0)_{s,0}$ and $A(R=100)_{s,0}$ are the average terms, $A(R=0)_{s,n}$ and $A(R=100)_{s,n}$ are the Fourier coefficients of the amplitude, $Y(R=0)_{s,n}$ and $Y(R=100)_{s,n}$ are the Fourier coefficients of the phase, where $n=1, 2,\ldots,144$ is the harmonic number, $T=288$ is the fundamental period corresponding to a "virtual year", and t is the time in hours: $t=0$ stands for 00:00 LT in January and $t=287$ stands for 23:00 LT in December. It is worthwhile specifying that the Fourier synthesis using only coefficients relative to the twelve dominant harmonics (out of 144) is enough to generate the time series $\Omega(t, R=0)_s$ and $\Omega(t, R=100)_s$ with an acceptable level of accuracy. This means that in (3a–3b) the summation is actually calculated only on a subset $n=\{k\}$ of harmonics, where k correspond to the twelve dominant harmonics.

4. Hypothesis of linear relationship between the Fourier coefficients and R. Calculating the angular coefficient and the intercept of the straight line joining the points of known coordinates $[(R=0, A(R=0)_{s,0}); (R=100, A(R=100)_{s,0})]$, $[(R=0, A(R=0)_{s,n}); (R=100, A(R=100)_{s,n})]$, $[(R=0, Y(R=0)_{s,n}); (R=100, Y(R=100)_{s,n})]$, the terms $a_{s,0}$, $b_{s,0}$, $a_{s,n}$, $b_{s,n}$, $c_{s,n}$ and $d_{s,n}$ are obtained and the following empirical models are defined:

$$\begin{aligned} A(R)_{s,0} &= a_{s,0}R + b_{s,0}, \\ A(R)_{s,n} &= a_{s,n}R + b_{s,n}, \\ Y(R)_{s,n} &= c_{s,n}R + d_{s,n}. \end{aligned} \tag{4}$$

Relationships (4) provide the Fourier coefficients at a given ionospheric station for any value of R.

5. Linear regression between terms $a_{s,0}$, $b_{s,0}$, $a_{s,n}$, $b_{s,n}$, $c_{s,n}$, $d_{s,n}$ and the geographic latitude ϕ_s of the ionospheric stations. This leads to define terms a_0^1, a_0^2, b_0^1, b_0^2, a_n^1, a_n^2, b_n^1, b_n^2, c_n^1, c_n^2, d_n^1, d_n^2, and consequently the following empirical models:

$$\begin{aligned} a_0 &= a_0^1\phi + a_0^2, \\ b_0 &= b_0^1\phi + b_0^2, \\ a_n &= a_n^1\phi + a_n^2, \\ b_n &= b_n^1\phi + b_n^2, \\ c_n &= c_n^1\phi + c_n^2, \\ d_n &= d_n^1\phi + d_n^2. \end{aligned} \tag{5}$$

It is worthwhile highlighting that, thanks to (5), in (4) the dependence of Fourier coefficients on the ionospheric station disappears and so it is possible to use (5) to get the amplitude and phase Fourier coefficients as a function of any solar activity and geographic latitude according to the following formulas:

$$\begin{aligned} A(R)_0 &= (a_0^1\phi + a_0^2)R + (b_0^1\phi + b_0^2), \\ A(R)_n &= (a_n^1\phi + a_n^2)R + (b_n^1\phi + b_n^2), \\ Y(R)_n &= (c_n^1\phi + c_n^2)R + (d_n^1\phi + d_n^2). \end{aligned} \tag{6}$$

Consequently, the SIRM prototype prediction algorithm in its extended form is:

$$\begin{aligned} \Omega(t, R, \phi) = {} & \left(a_0^1\phi + a_0^2\right)R + \left(b_0^1\phi + b_0^2\right) \\ & + \sum_{n=\{k\}} \left[\left(a_n^1\phi + a_n^2\right)R + \left(b_n^1\phi + b_n^2\right)\right] \sin\left[\frac{2\pi nt}{T} + \left(c_n^1\phi + c_n^2\right)R + \left(d_n^1\phi + d_n^2\right)\right], \end{aligned} \tag{7}$$

which provides yearly time series prediction of each key ionospheric characteristic with only $4 + 12{\cdot}8 = 100$ dominant coefficients, at a given location and time, by using as input a value of the solar index R.

6. Linear regression with the geographic longitude is not considered.

2.3 The SIRM Prototype: Some Examples

First SIRM prototype results (Zolesi et al. 1993) clearly demonstrated apparent linear trends between Fourier coefficients calculated by (4) for two levels of solar activity ($R = 0$ and $R = 100$) at each ionospheric station, and the geographic latitude of ionospheric stations, for three ionospheric characteristics: *fo*F2, *M*(3000)F2, and *h*'F. These results, partially represented in Fig. 2, confirmed the basic assumption that A_n and Y_n can be represented as linearly dependent on the geographic latitude as expressed by (6).

While the Fourier synthesis reproduces exactly the time series $\Omega(t,\ R = 0)_s$ and $\Omega(t,\ R = 100)_s$ when $n = 144$, stopping the Fourier synthesis at $n = \{k\}$ presents a serious question about whether 100 numerical coefficients are enough to provide a good representation of the yearly time series.

In this regard, especially during winter months, the results of Fig. 3 for Rome and Poitiers ionospheric stations show a good agreement between the *fo*F2 monthly median values

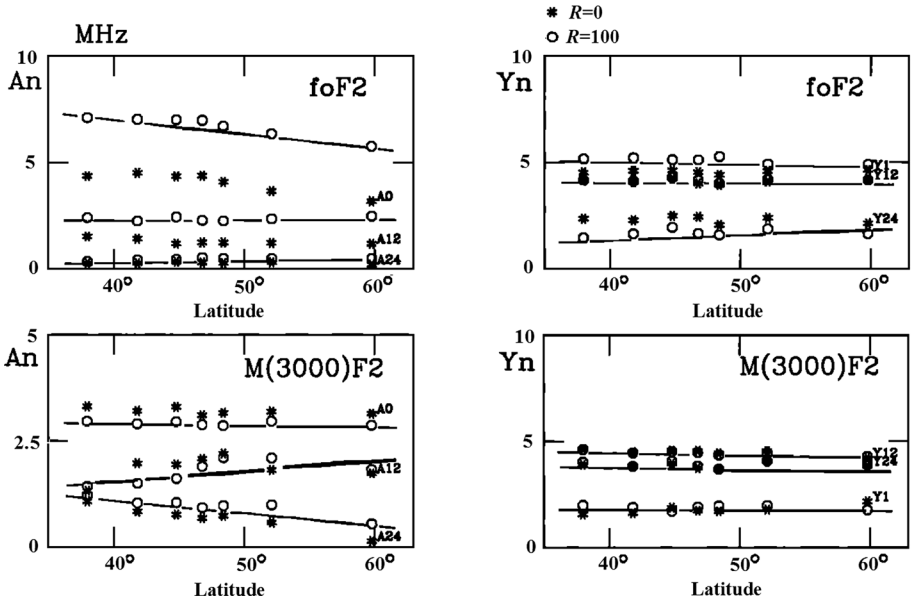

Fig. 2 Linear trends of some selected Fourier coefficients A_n and Y_n vs latitude for two levels of solar activity: $R=0$ and $R=100$. A_{12} and A_{24} for *fo*F2 and $M(3000)F2$ are multiplied by 10 [re-elaborated from Zolesi et al. (1993)]

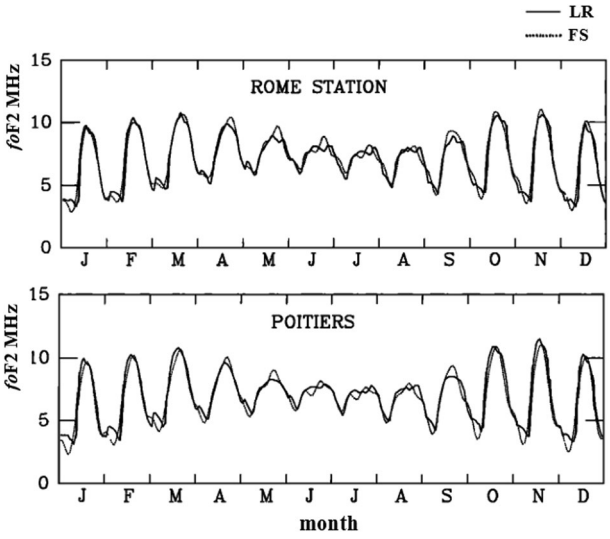

Fig. 3 Yearly predictions of *fo*F2 monthly median values calculated with (thick curve) the simple linear regression model (2) and with (light curve) the Fourier synthesis (7) at Rome (12.5° E, 41.9° N) and Poitiers (0.3° E, 46.6° N) ionospheric stations for $R=100$ [re-elaborated from Zolesi et al. (1993)]

generated by the Fourier synthesis (7) and the *fo*F2 time series calculated by the linear regression (2).

Once verified that the SIRM prototype could reliably reproduce data used for its development, it was tested at Dourbes (4.6° E, 50.1° N), an ionospheric station not included in the historical database employed to develop the model. From the comparison between

SIRM prototype predictions and observations recorded at Dourbes emerged that the model can satisfactorily reproduce the ionospheric characteristics except for *fo*F1 (Zolesi et al. 1993).

Although the SIRM prototype was initially developed as a prediction algorithm to be used over the mid-latitude European region, it can be successfully applied over any relatively narrow region in longitude including an adequate number of ionosonde stations with a relatively long and reliable historical database of ionospheric characteristics.

Accordingly, the SIRM prototype was applied in four different mid-latitude sectors of the world: North-East of North America, North-East Asia, South-East of South America, and South-East Australia (see Fig. 4).

From *fo*F2 and *M*(3000)F2 data recorded from 1967 to 1976 at the ionospheric stations listed in Table 2, collected by the World Data Center-A (Boulder, Colorado), 100 numerical coefficients relative to each of the regions represented in Fig. 4 were calculated and used as input to generate *fo*F2 and *M*(3000)F2 monthly median values.

As input parameter to generate *fo*F2 and *M*(3000)F2 predictions over the four regions shown in Fig. 4, the 12-month running mean R_{12} of the monthly sunspot number was considered in place of *R* (Kouris et al. 1993). Similarly to the European region, also in these regions Fourier coefficients and geographic latitudes of the involved ionospheric stations show a linear trend (Zolesi et al. 1996). In particular, the decreasing trend of the amplitude Fourier coefficients with the latitude, observed for the ionospheric characteristic *fo*F2, confirms the reliability of the SIRM prototype. Moreover, tests carried out at Kokubunji, considering data recorded in years not included in the database used to generate the numerical

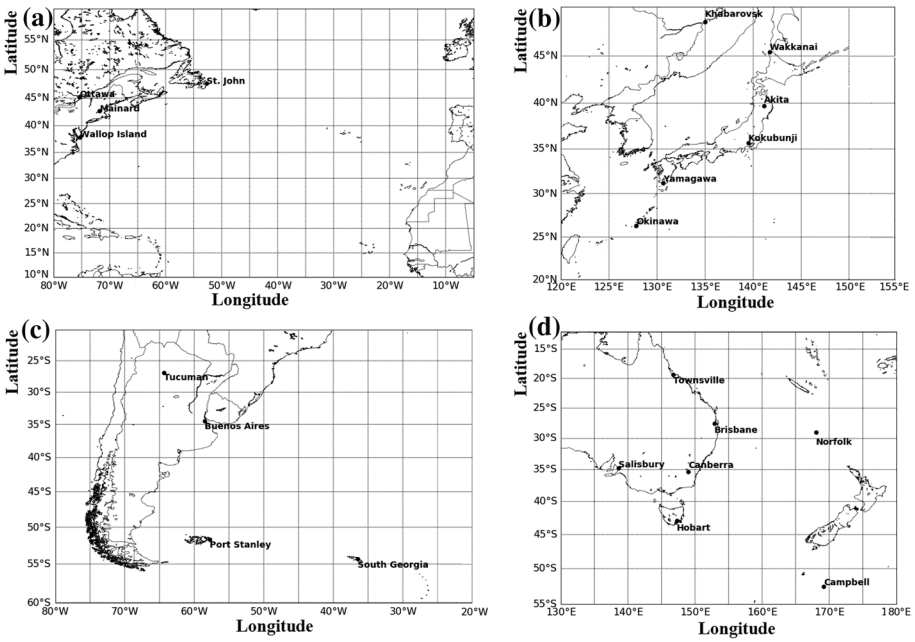

Fig. 4 The four regions where the SIRM prototype was applied: **a** North-East of North America; **b** North-East Asia; **c** South-East of South America; **d** South-East Australia. The position of the ionospheric stations for which the datasets were used to get the numerical coefficients are also shown

Table 2 Ionospheric stations considered to develop the SIRM prototype over the four regions represented in Fig. 4

Station	Geographic longitude	Geographic latitude	Years of available data
North-East of North America			
St. John's	52.7° W	47.6° N	1967–1976
Ottawa	75.41° W	45.4° N	1967–1976
Mainard	71.8° W	42.7° N	1967–1976
Wallops Island	75.5° W	37.9° N	1967–1976
South-East of South America			
South Georgia	36.5° W	54.3° S	1967–1976
Port Stanley	57.8° W	51.7° S	1967–1976
Buenos Aires	58.5° W	34.5° S	1967–1976
Tucuman	64.4° W	26.9° S	1967–1976
North-East Asia			
Khabarovsk	135.0° E	48.5° N	1967–1976
Wakkanai	141.7° E	45.4° N	1967–1976
Akita	141.1° E	39.7° N	1967–1976
Kokubunji	139.5° E	35.7° N	1967–1976
Yamagawa	130.6° E	31.2° N	1967–1976
Okinawa	127.8° E	26.3° N	1967–1976
South-East Australia			
Campbell	169.2° E	52.5° S	1967–1976
Hobart	147.3° E	42.9° S	1967–1976
Canberra	149.0° E	35.3° S	1967–1976
Salisbury	138.6° E	34.7° S	1967–1976
Norfolk Island	168.0° E	29.0° S	1967–1976
Brisbane	152.9° E	27.5° S	1967–1976
Townsville	146.7° E	19.3° S	1967–1976

coefficients, have shown an acceptable agreement between measurements and modelled values for both *fo*F2 and *M*(3000)F2 (Zolesi et al. 1996). Examples of *fo*F2 and *M*(3000)F2 maps generated by the SIRM prototype over the four regions of Fig. 4 are shown in Fig. 5.

An attempt to apply the SIRM prototype to the Antarctic region was also made, but it did not give good results. The main reason behind this unsuccessful test is that the model is very sensitive to the quality of the dataset considered to derive the coefficients. At high latitudes monthly median values of the ionospheric characteristics are often calculated on a small number of measurements. In addition, there are strong doubts about the quality of measurements themselves, especially in the Antarctic region, for which the ionograms are often very hard to be validated.

From the considerations made so far, it clearly emerges that the SIRM prototype provides a good output in different mid-latitude parts of the world. At the same time, thanks to the fact that it is represented by only 100 numerical coefficients, it satisfies the request of relatively short calculation times for computers in use in the early 1990s. It is worthwhile highlighting that 100 is a small number if compared with the 988 numerical coefficients for *fo*F2 and the 441 numerical coefficients for *M*(3000)F2 characterizing the global model developed by Jones and Gallet (1962, 1965) to generate CCIR maps of *fo*F2 and *M*(3000)

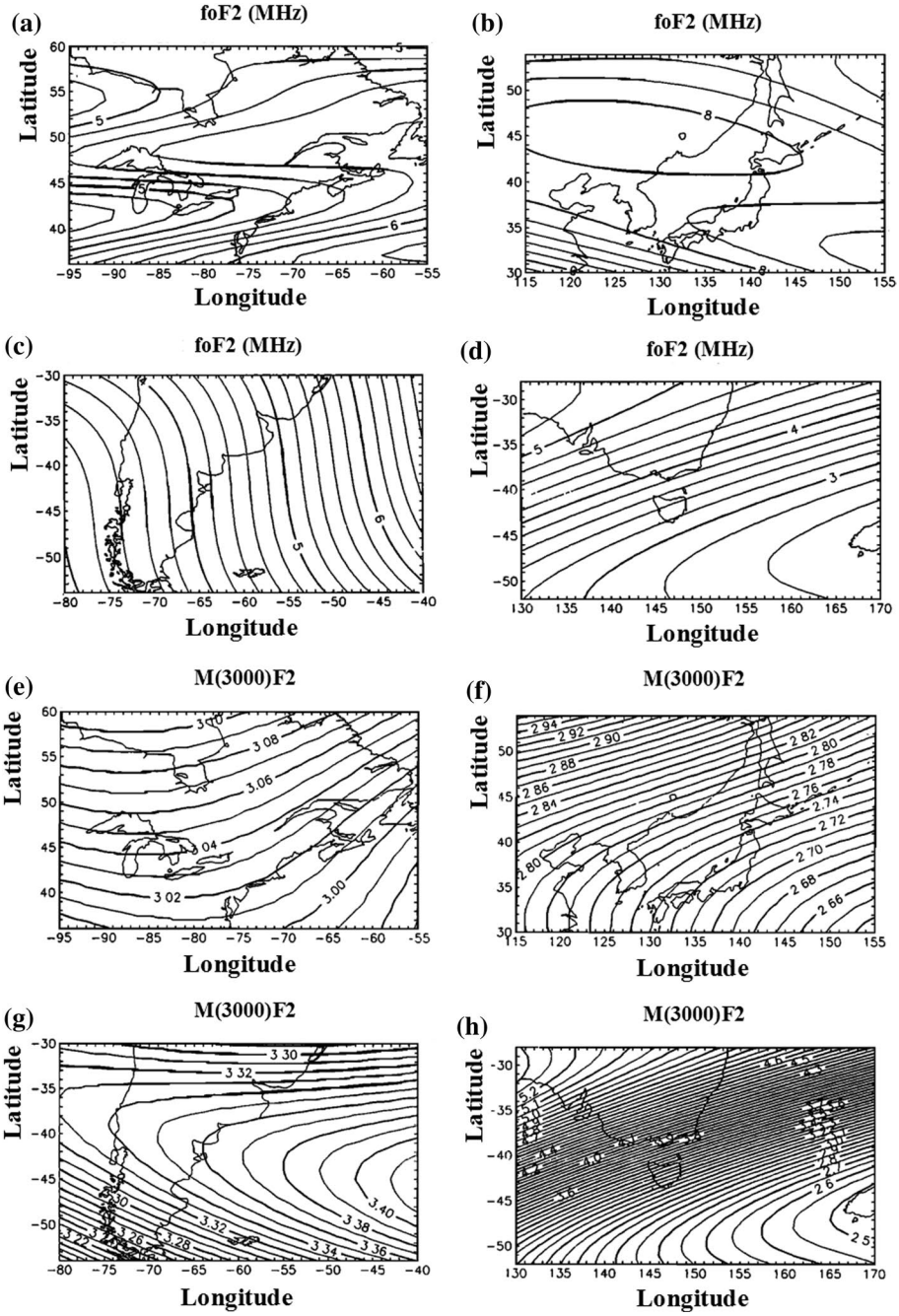

Fig. 5 **a**–**d** *fo*F2 maps and **e**–**h** *M*(3000)F2 maps generated over **a**, **e** North-East of North America, **b**, **f** North-East Asia, **c**, **g** South-East of South America, and **d**, **h** South-East Australia [re-elaborated from Zolesi et al. (1996)]

F2 monthly median values. In the light of these results, the authors have been encouraged to further improve the prototype as it will be described in detail in the next Section.

3 SIRM Prototype Improvements

The SIRM prototype showed the following shortcomings: (1) the use of only 12 dominant Fourier coefficients out of 144 available did not reproduce effectively the yearly time series during summer months; (2) phase Fourier coefficients were not corrected to consider the displacement of each reference station with respect to the central meridian of the corresponding time zone; (3) the use of the monthly mean solar sunspot number R was not the best choice. With regard to this matter Kouris et al. (1993), in the framework of COST 238, suggested that it would be preferable to use R_{12} (the 12-month running mean of the monthly sunspot number); (4) it was based on a relatively small number of ionospheric stations not uniformly distributed in the area under consideration; (5) among these stations there were some (Gibilmanna, Lannion, De Bilt, and Uppsala) for which data were available only for a very limited number of years. In this regard, Fig. 6 shows the data availability of each ionospheric station involved in the development of the SIRM prototype with respect to the solar activity cycle.

This is why an improvement of the SIRM prototype was accomplished in the framework of the COST Action 251. The correction of the phase Fourier coefficients will be described in detail in the Appendix 1.1. Differently from the SIRM prototype, the improved SIRM algorithm was developed only for the ionospheric characteristics *fo*F2 and *M*(3000)F2. Ionospheric stations that sounded only for a few years and those characterized by either too fragmented records or large gaps of data were discarded. So doing, *fo*F2 and *M*(3000)F2 hourly monthly median values of good quality, recorded at 12 reference ionospheric stations (see Table 3), constituted the new and larger database

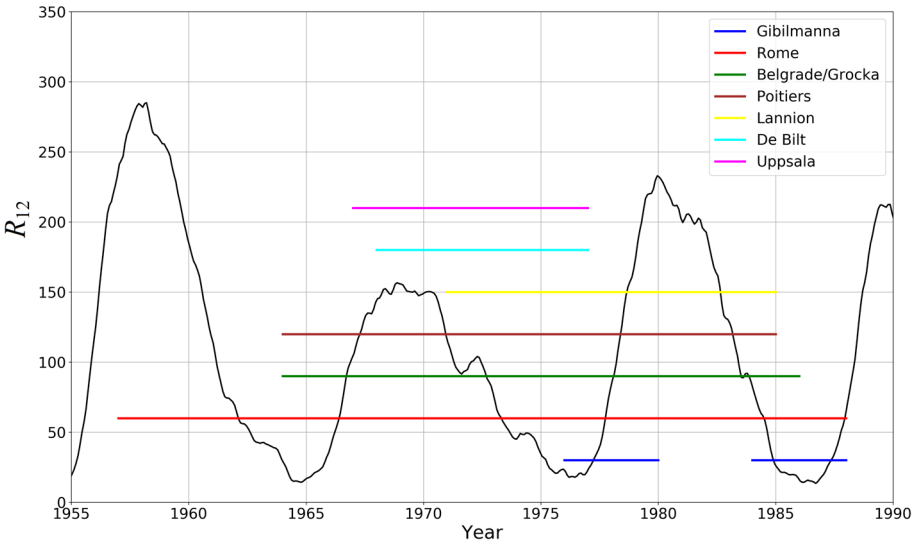

Fig. 6 The data availability of each ionospheric station involved in the development of the SIRM prototype is shown overlapped to the R_{12} curve from 1955 to 1990

Table 3 (bold) Ionospheric stations used to calculate the improved SIRM coefficients and (italics) ionospheric stations chosen to test the procedure

Station name	Geographic longitude	Geographic latitude	Years of available data
Arkangelsk	**40.5° E**	**64.4° N**	**1969–1993**
Ashkhabad	**58.3° E**	**37.9° N**	**1957–1987, 1988–1998**
Athens	*23.6° E*	*38.0° N*	*1961–1974, 1976, 1983, 1987*
Belgrade/Grocka	*20.5° E*	*44.8° N*	*1985–1993*
De Bilt	**5.2° E**	**52.1° N**	**1957–1960, 1971–1981**
Dourbes	**4.6° E**	**50.1° N**	**1957–1997**
El Arenosillo	*6.8° W*	*37.1° N*	*1975–1979, 1982–1985, 1993–1997*
Gibilmanna	**14.0° E**	**37.6° N**	**1976–1980, 1983–1995**
Gorki	*44.2° E*	*56.1° N*	*1959–1989, 1992*
Kaliningrad	**20.6° E**	**54.7° N**	**1964–1994**
Kiev	**30.5° E**	**50.5° N**	**1964–1976, 1978–1992**
Lannion	**3.4° W**	**48.7° N**	**1961–1994, 1996–1997**
Lerwick	*1.2° W*	*60.1° N*	*1995–1998*
Lisbon	*9.2° W*	*38.8° N*	*1987–1992*
Lycksele	*18.8° E*	*64.6° N*	*1957–1998*
Murmansk	*33.0° E*	*69.0° N*	*1957–1962, 1964–1977, 1981–1984, 1986, 1989–1994*
Nicosia	*33.2° E*	*35.1° N*	*1992, 1995–1997*
Poitiers	**0.3° E**	**46.6° N**	**1957–1960, 1964–1998**
Rome	**12.5° E**	**41.9° N**	**1958–1972, 1976–1998**
Slough (Chilton)	**0.6° W**	**51.5° N**	**1931–1998**
South Uist	*7.3° W*	*57.4° N*	*1969–1990*
St Peter Ording	*8.6° E*	*54.3° N*	*1983–1992*
Tbilisi	*44.8° E*	*41.7° N*	*1963–1986*
Tromso	*19.0° E*	*69.7° N*	*1958, 1994*
Uppsala	**17.6° E**	**59.8° N**	**1957–1998**

used to recalculate the SIRM numerical coefficients (COST 251 VI Ionospheric Database on CD-ROM 1999, provided on request by the Rutherford and Appleton Laboratory). It is worth noting that in the past there was no internationally agreed procedure for testing ionospheric mapping methods. However, in the framework of COST action 251, an impartial team of researchers was formed to assess the validity of the newly developed SIRM with respect to global models recommended by CCIR, now known as the International Telecommunication Union (ITU-R). The rigid protocol established by the management committee required that the testing procedures had to be performed over the COST 251 area, extending in longitude from 10° W to 60° E and in latitude from 35° N to 70° N (Fig. 7), using the index R_{12} as representative of the solar activity. Therefore, months of low and high solar activity were selected for three seasons and for four different hours. A rigorous quality check was also adopted (see Hanbaba 1999 for more details), after which 40,354 samples for *fo*F2 and 33,251 samples for *M*(3000)F2 were selected. Performances of both ITU-R and improved SIRM were then calculated in terms of root mean square error (rmse) (Hanbaba 1999). Results showed that the

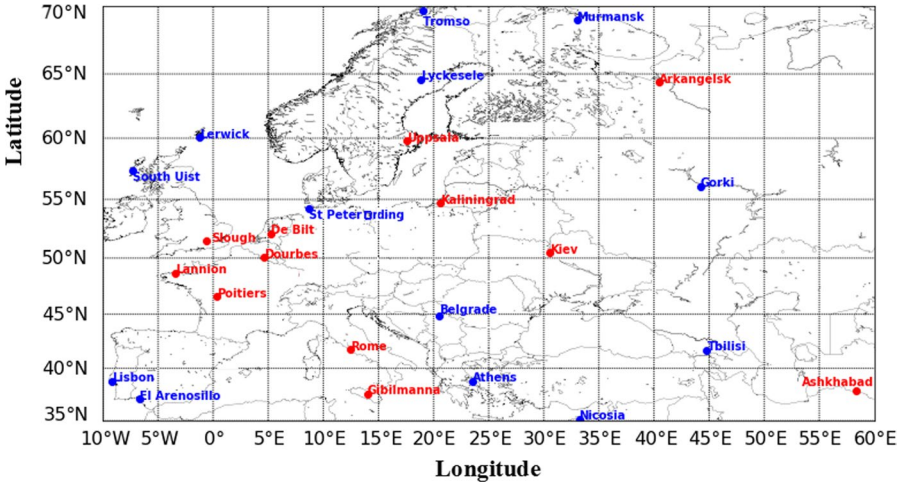

Fig. 7 The COST 251 Action region showing (in red) the ionospheric stations considered to recalculate the model coefficients and (in blue) ones considered for testing

improved SIRM was slightly better than the ITU-R global model for what concerns the ionospheric characteristic *fo*F2 ($\text{rmse}_{\text{SIRM}} = 0.610$ MHz vs. $\text{rmse}_{\text{ITU-R}} = 0.635$ MHz), while for the characteristic $M(3000)$F2 the two models were practically equivalent ($\text{rmse}_{\text{SIRM}} = 0.114$ vs. $\text{rmse}_{\text{ITU-R}} = 0.116$) (Hanbaba 1999). Table 3 shows the reference ionospheric stations chosen to improve the SIRM prototype and those employed in the testing procedure. The arrangement of reference and testing ionospheric stations, positioned within the COST 251 area, is shown in Fig. 7. It is worth pointing out that the coefficients of the improved SIRM model derive mainly from ionospheric stations that are inside the region extending in longitude from 5° W to 40° E and in latitude from 34° N to 60° N, which is therefore considered the validity area of the SIRM model.

The historical data of *fo*F2 and $M(3000)$F2 collected in the ionospheric stations listed in Table 3, and the use of R_{12} instead of R, are the main "ingredients" through which the Fourier coefficients have been recalculated. It is worth highlighting that Fourier coefficients in the improved SIRM are calculated on a monthly basis and no more on a yearly basis. This means that now the Fourier synthesis, with twelve coefficients, can exactly reproduce the monthly time series of *fo*F2 and $M(3000)$F2. Therefore, in this case

$$\Omega\left(t, R_{12}, m\right)_s = A\left(R_{12}, m\right)_{s,0} + \sum_{n=1}^{12} A\left(R_{12}, m\right)_{s,n} \sin\left(\frac{2\pi nt}{T} + Y\left(R_{12}, m\right)_{s,n}\right), \qquad (8)$$

where m is the month of the year.

As consequence, the improved SIRM is fully represented by two set of 1200 (100×12) numerical coefficients, one for *fo*F2 and the other one for $M(3000)$F2. To this regard a detailed mathematical description of the improved SIRM model, along with an example of numerical coefficients used as input parameters to predict *fo*F2 hourly monthly median values in January, are given in the Appendix 1.2.

3.1 Applications of the Improved SIRM

The main applications of the improved SIRM model (hereafter referred simply as SIRM model) in the framework of several international research projects can be briefly summarized as follows:

a. In the framework of GIFINT (Geomagnetic Indices Forecasting and Ionospheric Nowcasting Tools), a pilot project funded by the European Space Agency, long-term prediction maps of *fo*F2 and *M*(3000)F2 over the central Mediterranean region, from 5° E to 20° E in longitude and from 34° N to 48° N in latitude, are provided applying the SIRM model when autoscaled data from Rome and Gibilmanna are simultaneously unavailable. They are generated every hour, and can be found at the following sites: http://ionos.ingv.it/gifint/fof2.htm and http://ionos.ingv.it/gifint/m3000f2.htm. An example of these maps is given in Fig. 8 for July 2019 at 10:00 UT.
b. The SIRM output is fully applied in two important projects funded by the European Community: DIAS (DIgital upper Atmosphere Server; http://www.iono.noa.gr/DIAS/) (Belehaki et al. 2005, 2015) and ESPAS (near-Earth SPAce data infraStructure for e-Science; http://www.espas-fp7.eu/) (Belehaki et al. 2016). ESPAS is a portal providing access to several space-physics data archives, and among these the one produced in the framework of DIAS. Within several products offered in the framework of the DIAS project, there are the long-term prediction maps of *fo*F2 and *M*(3000)F2 derived by the SIRM procedure applied on a grid extending in longitude from 5° W to 40° E and in latitude from 34° N to 60° N. An example of *fo*F2 and *M*(3000)F2 maps made available by the DIAS system is given in Fig. 9 for July 2019 at 13:00 UT.
c. MUF and skip distance long-term prediction maps are an additional product made available by the DIAS system. They are generated on the basis of both the SIRM model and the formula developed by Lockwood (1983) for the calculation of the MUF. The maps are centred over 11 different European ionospheric stations: El Arenosillo (6.8° W, 37.1° N), Athens (23.6° E, 38.0° N), Madrid (3.4° W, 40.2° N), Roquetes (Ebre) (0.5° E, 40.8° N), Rome (12.5° E, 41.9° N), Pruhonice (14.6° E, 50.0° N), Chilton (0.6° W, 51.5° N), Juliusruh (13.4° E, 54.6° N), Moscow (37.3° E, 55.5° N), Stockholm (18.3° E, 59.2° N), and Lyckesele (18.8° E, 64.6° N). Figure 10 shows some examples of MUF and skip distance long-term prediction maps for four different transmitting points in July 2019 at 06:00 UT.

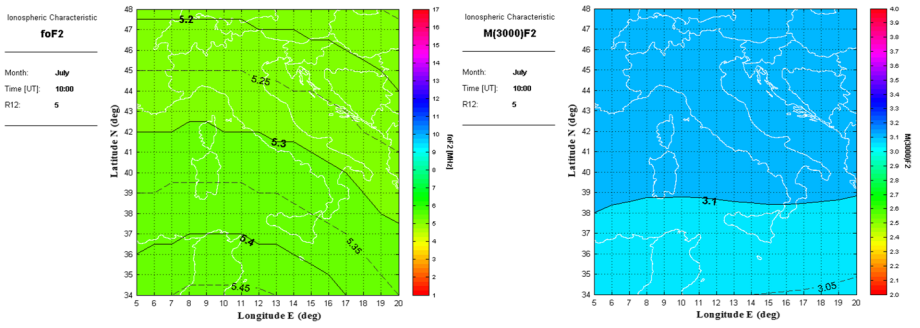

Fig. 8 Long-term prediction maps of (left) *fo*F2 and (right) *M*(3000)F2 over the central Mediterranean area (Italy) for July 2019 at 10:00 UT using as input an expected value of $R_{12}=5$

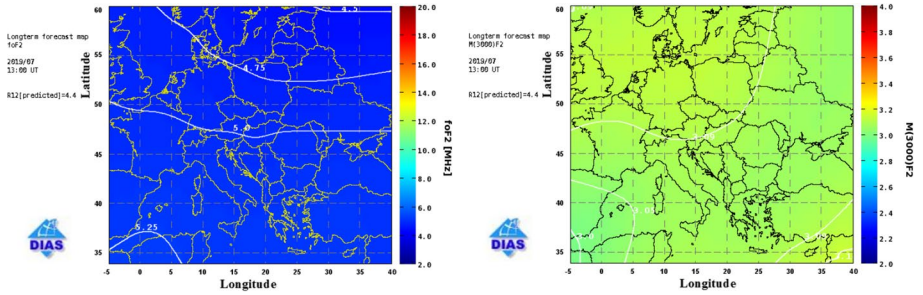

Fig. 9 Long-term prediction map of (left) *fo*F2 and (right) *M*(3000)F2 over the European region covered by the DIAS project in July 2019 at 13:00 UT, corresponding to an expected value of $R_{12}=4.4$

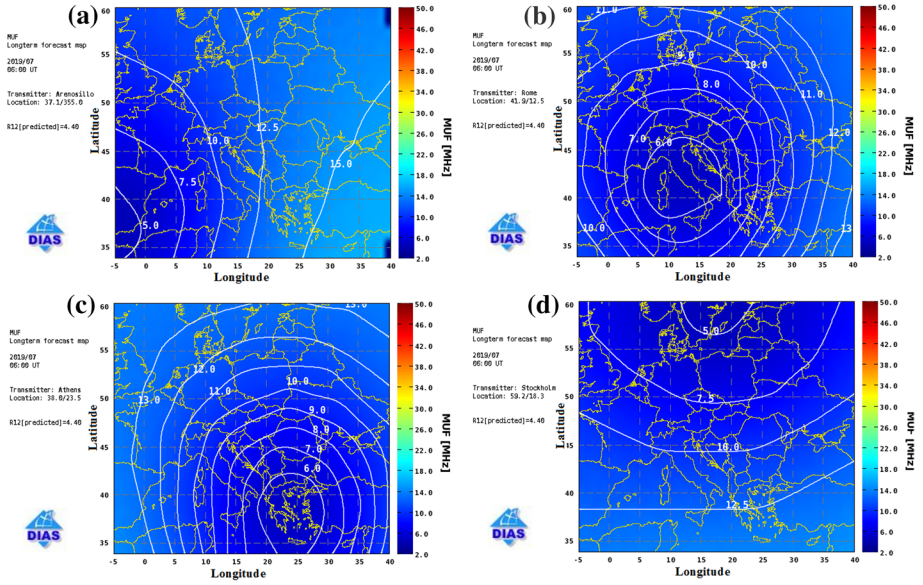

Fig. 10 MUF and corresponding skip distance long-term prediction maps in July 2019 at 06:00 UT, corresponding to an expected value of $R_{12}=4.4$, and centred on four different transmitting points: **a** El Arenosillo; **b** Rome; **c** Athens; **d** Stockholm

d. Thanks to an original software tool developed at INGV, in the framework of the Space Situational Awareness (SSA) Programme P2-SWE-1 funded by ESA (http://swe.ssa.esa.int/web/), *fo*F2 long-term numerical grids were generated to expand the DIAS prediction capabilities to high European latitudes. For this purpose, three different zones were considered: a north one (80° N–61° N) where only the CCIR global model is applied (Jones and Gallett 1962, 1965); a south one (49° N–34° N) where only the SIRM model is applied; a buffer zone (60° N–50° N) where both CCIR and SIRM are applied giving a suitable weight to the prediction according to the latitude under consideration (Pietrella 2015). Graphical procedures were then applied to generate corresponding maps of *fo*F2

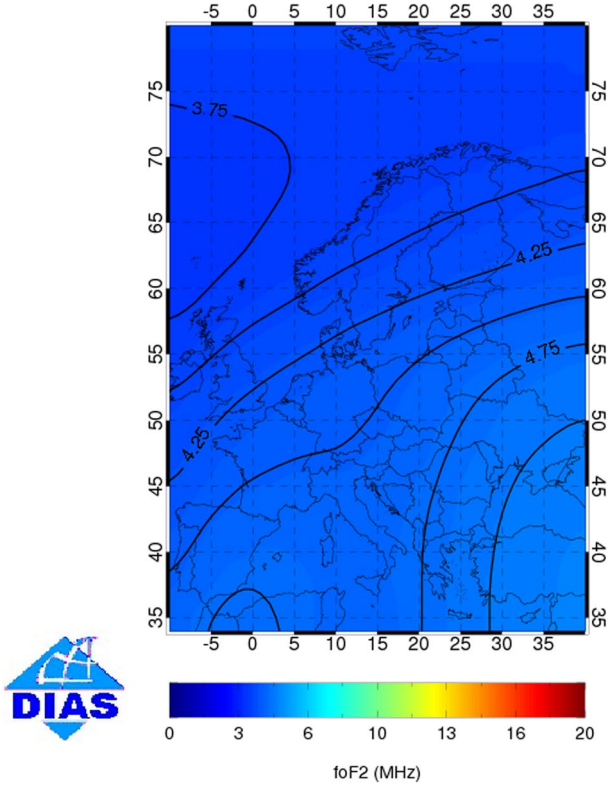

Fig. 11 Example of *fo*F2 long-term prediction map developed in the framework of the ESA SSA Programme P2-SWE-1. The map refers to July 2019 at 07:00 UT and corresponds to an expected value of $R_{12}=4.4$

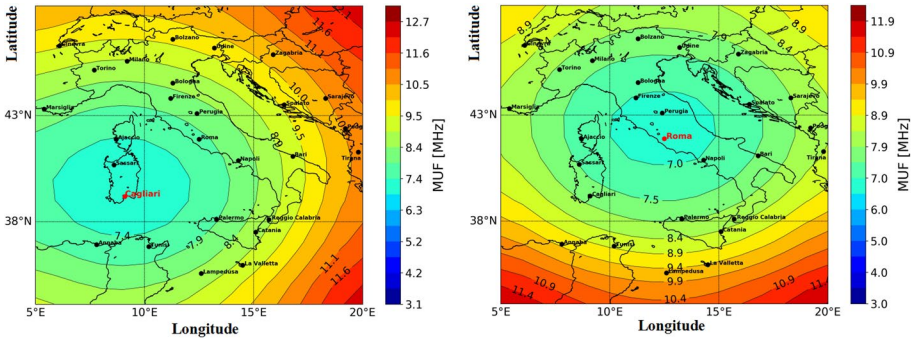

Fig. 12 MUF and corresponding skip distance long-term predictions maps over Italy centred on (left) Cagliari and (right) Rome, in March 2019 at 12:00 UT, corresponding to an expected value of $R_{12}=5.5$

extended in longitude from 10° W to 40° E and in latitude from 34° N to 80° N. An example of these maps is given in Fig. 11 in July 2019 at 07:00 UT.

e. A procedure to get MUF and skip distance long-term predictions maps over Italy based on the SIRM model has been recently developed (Pietrella and Pezzopane 2020). Figure 12 shows two examples in March 2019 at 12:00 UT: one centred on Cagliari (9.1° E, 39.2° N) in western Italy and another one centred on Rome (12.5° E, 41.9° N) in central Italy.

f. In the framework of the Cyprus Ionospheric Forecasting Service project, co-funded by the Ministry of Cypriot Defence and the European fund for the regional development, a very extensive database of numerical grids of long-term predictions of *fo*F2 and *M*(3000)F2 and MUF has been calculated in the East region of the Mediterranean extending in longitude from 20° E to 45° E and in latitude from 30° N to 40° N.

4 The SIRM UPdated (SIRMUP) Procedure

As already mentioned in the introduction, SIRM was developed for long-term predictions providing monthly median maps of *fo*F2 and *M*(3000)F2, which represent the prevailing ionospheric conditions. However, during geomagnetic and ionospheric storms the climatological picture provided by SIRM cannot describe adequately the real-time behaviour of the ionosphere. In such cases, a nowcasting model is required. This is why in the early years of 2000 a procedure was developed to update SIRM median prediction maps with measured data from Digisonde Portable Sounders (DPS4) equipped with the Automatic Real-Time Ionogram Scaler with True–height (ARTIST) system (Reinisch and Huang 1983; Reinisch et al. 2005; Galkin and Reinisch 2008), which regularly operated in four European reference ionospheric stations at that time: Athens, Rome, Chilton, and Juliusruh (Fig. 13a). This procedure was called SIRMUP (Zolesi et al. 2004).

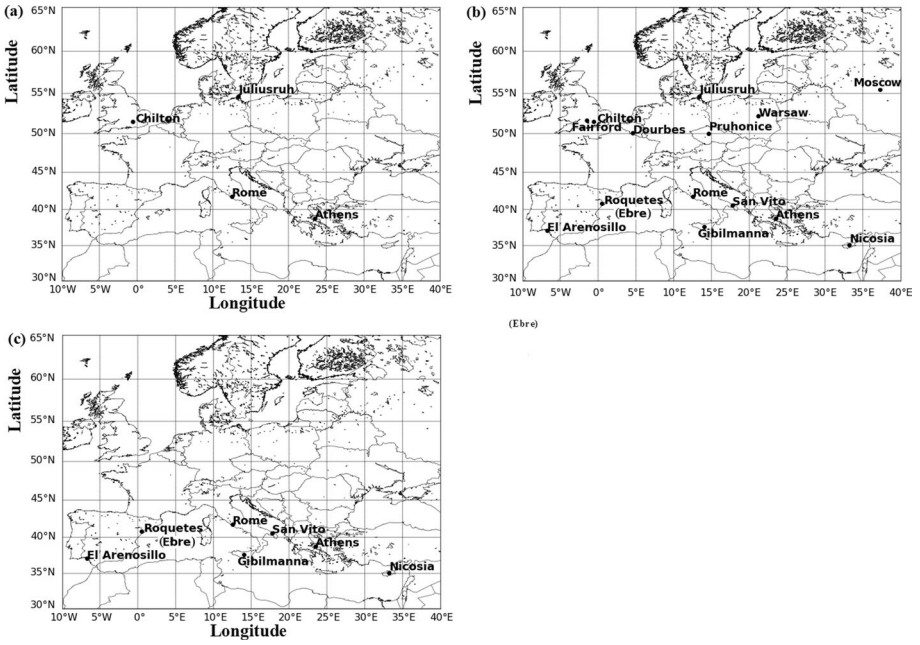

Fig. 13 Ionospheric reference stations over the European region which: **a** were initially used to update the SIRM procedure; **b** can be nowadays used for the real-time SIRM updating; **c** can be potentially used for updating the SIRM procedure over the Mediterranean area

The proposed technique calculates, at reference ionospheric stations, residuals between ionosonde autoscaled measurements and model predictions obtained for different values of the solar activity index, to find the minimum residual and hence the corresponding "effective" solar activity index (Houminer et al. 1993).

Specifically, an effective value $R_{12\text{eff}}$ of R_{12} is obtained as the one minimizing the mean square error

$$\Delta = \frac{1}{n}\sum_{i=1}^{n}\left(X_{\text{aut},i} - X_{\text{mod},i}\right)^2 \tag{9}$$

between autoscaled $X_{\text{aut},i}$ and modelled $X_{\text{mod},i}$ values of the ionospheric characteristic at the reference station i, where n is the number of reference ionospheric stations.

Typically, X stands for foF2 or M(3000)F2, which means that in principle two different $R_{12\text{eff}}$ are obtained: $R_{12\text{eff}}(fo\text{F2})$ and $R_{12\text{eff}}(M(3000)\text{F2})$.

The SIRMUP procedure is nothing but the SIRM that uses $R_{12\text{eff}}$ instead of R_{12}, being $R_{12\text{eff}}$ a more suitable index for nowcasting purposes, as highlighted by both Zolesi et al. (2004) and Tsagouri et al. (2005). SIRMUP was tested considering two geomagnetic storm periods: one characterized by moderately disturbed ionospheric conditions, and the other one characterized by strong ionospheric disturbances with daytime positive effects and prolonged negative effects. At the same time, a quiet geomagnetic period characterized by large-scale daytime positive ionospheric effects was also considered in the testing procedure. Results demonstrated that SIRMUP is always better than SIRM: during storm periods, with an increase of accuracy of 80% and 40% for foF2 and M(3000)F2, respectively; for quiet conditions with an increase of accuracy of 40% and 22% for foF2 and M(3000)F2, respectively. This means that SIRMUP provides a satisfactory real-time specification of the ionosphere, which is relevant for improving the quality of HF telecommunication systems especially during severe disturbed conditions.

Nowadays, after about 20 years from the early stage of SIRMUP development, the number of reference ionospheric stations capable to provide autoscaled data in the European area has remarkably increased passing from four to fourteen: Moscow, Juliusruh, Warsaw (21.2° E, 52.2° N), Fairford (1.5° W, 51.7° N), Chilton, Dourbes, Pruhonice, Rome, San Vito (17.8° E, 40.6° N), Roquetes (Ebre), Athens, Gibilmanna, El Arenosillo, and Nicosia (Fig. 13b). Corresponding autoscaled data are provided by ARTIST, except for: Rome and Gibilmanna where the ionograms are recorded by the AIS-INGV ionosonde (Zuccheretti et al. 2003) and autoscaled by the Autoscala system (Pezzopane and Scotto 2005, 2007; Scotto 2009); Warsaw where the ionograms are recorded by the VISRC2 ionosonde (Pezzopane et al. 2009) equipped with Autoscala. This is a great advantage offering the possibility to always calculate a value of $R_{12\text{eff}}$, and consequently to regularly update the SIRM procedure over Europe also when autoscaled data are unavailable from some ionospheric stations.

It should be noticed that SIRMUP can also be applied over an area relatively smaller than Europe; for example, over the Mediterranean region with the following seven ionospheric stations: Rome, Roquetes (Ebre), San Vito, Athens, Gibilmanna, El Arenosillo, and Nicosia (Fig. 13c). In principle, if at a given epoch autoscaled data are simultaneously available for each station, the calculation of $R_{12\text{eff}}$ is based on seven ionospheric stations, which is a number relatively high if compared with the size of the region under consideration. Moreover, Fig. 13c shows that the geographical distribution of the reference ionospheric stations is very satisfactory because they uniformly cover the west, central, and east part of the Mediterranean. These factors affect positively the accuracy of the real-time

updating method, which means that a very reliable value of $R_{12\text{eff}}$ can be calculated and then used for operational nowcasting applications over this restricted area.

Figure 14 shows a flowchart summarizing the main steps behind the SIRM and SIRMUP procedures.

4.1 Applications of the SIRMUP Procedure

A list of the main applications of the SIRMUP procedure are summarized as follows:

a. In the framework of the aforementioned GIFINT project, nowcasting maps of *fo*F2 and *M*(3000)F2 were provided applying SIRMUP. An example of these maps is given in Fig. 15, where SIRM is updated through values of $R_{12\text{eff}}(foF2) = +60$ and $R_{12\text{eff}}(M(3000)F2) = -15$ calculated with *fo*F2 and *M*(3000)F2 values autoscaled at the ionospheric stations of Rome (*fo*F2 = 6.40 MHz, *M*(3000)F2 = 3.19) and Gibilmanna (*fo*F2 = 6.70 MHz, *M*(3000)F2 = 3.13) on 22 March 2015 at 20:00 UT.
b. Nowcasting maps of *fo*F2 and *M*(3000)F2, as well as MUF and skip distance nowcasting maps centred over the eleven European ionospheric stations mentioned in Sect. 3.1, are some of the relevant products provided by the DIAS system for space weather purposes. They are generated applying respectively the SIRMUP procedure, and the SIRMUP procedure jointly with the Lockwood formula (Lockwood 1983), over a region

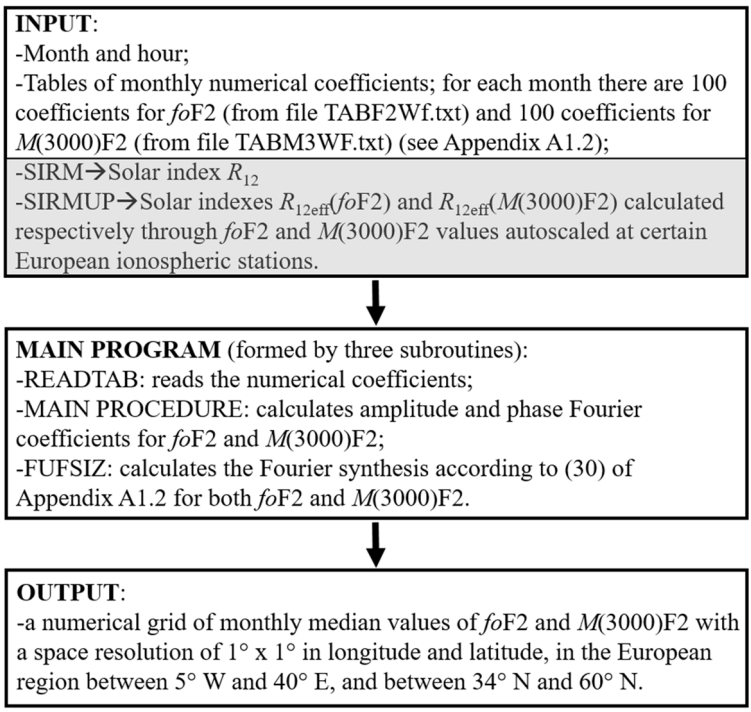

Fig. 14 Flowchart summarizing the main steps characterizing SIRM and SIRMUP. The difference between the two models stands on the considered solar activity index which for SIRM is R_{12}, while for SIRMUP are $R_{12\text{eff}}(foF2)$ and $R_{12\text{eff}}(M(3000)F2)$, as highlighted in grey in the flowchart

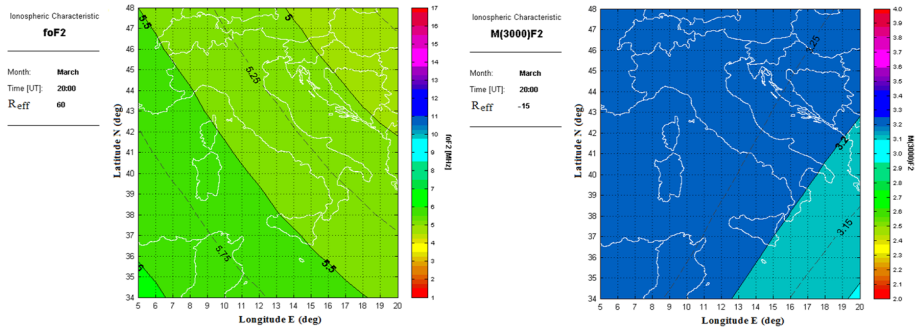

Fig. 15 Nowcasting maps of (left) *fo*F2 and (right) *M*(3000)F2 over the central Mediterranean area on 22 March 2015 at 20:00 UT

extending in longitude from 5° W to 40° E and in latitude from 34° N to 60° N. Figure 16 shows some examples of *fo*F2 and *M*(3000)F2 nowcasting maps corresponding to $R_{12\text{eff}}(fo\text{F2}) = 0$ and $R_{12\text{eff}}(M(3000)\text{F2}) = 30$, respectively. They are calculated exploiting the *fo*F2 and *M*(3000)F2 autoscaled values simultaneously available at the ionospheric stations of Juliusruh, Roquetes (Ebre), Dourbes and Pruhonice on 7 July 2019 at 13:00 UT. Examples of MUF and skip distance nowcasting maps for four transmitting points corresponding to $R_{12\text{eff}}(fo\text{F2}) = 0$ and $R_{12\text{eff}}(M(3000)\text{F2}) = 30$ calculated on 12 July 2019 at 06:00 UT are shown in Fig. 17.

c. In the framework of the previously mentioned SSA Programme P2-SWE-1, nowcasting numerical grids of *fo*F2 based on SIRMUP&CCIR method were generated to expand the DIAS prediction capabilities to high European latitudes (Belehaki et al. 2015). To this aim the following three steps were accomplished:

- the CCIR global model (Jones and Gallett 1962, 1965) is applied for the high-latitude zone (80° N–61° N), using as input the effective index $R_{12\text{eff}}(fo\text{F2})_{\text{high}}$ calculated on the basis of *fo*F2 autoscaled values recorded by the two high-latitude digisondes of Sodankyla (26.6° E, 67.4° N) and Tromso (19.0° E, 69.6° N).

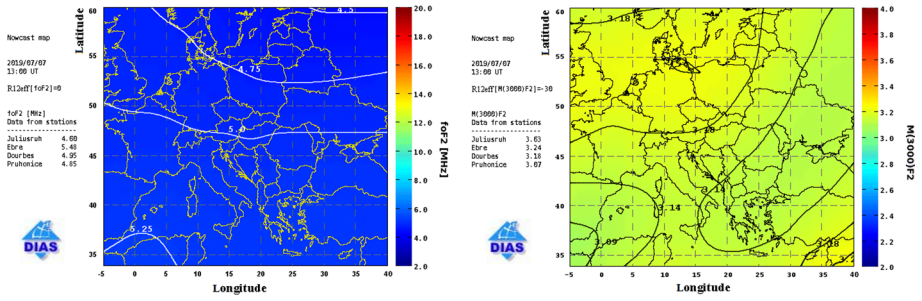

Fig. 16 Nowcasting maps of (left) *fo*F2 and (right) *M*(3000)F2 over the mid-latitude European region on 7 July 2019 at 13:00 UT. On the left side of each map the ionospheric stations involved in the calculation of $R_{12\text{eff}}(fo\text{F2})$ and $R_{12\text{eff}}(M(3000)\text{F2})$ are listed

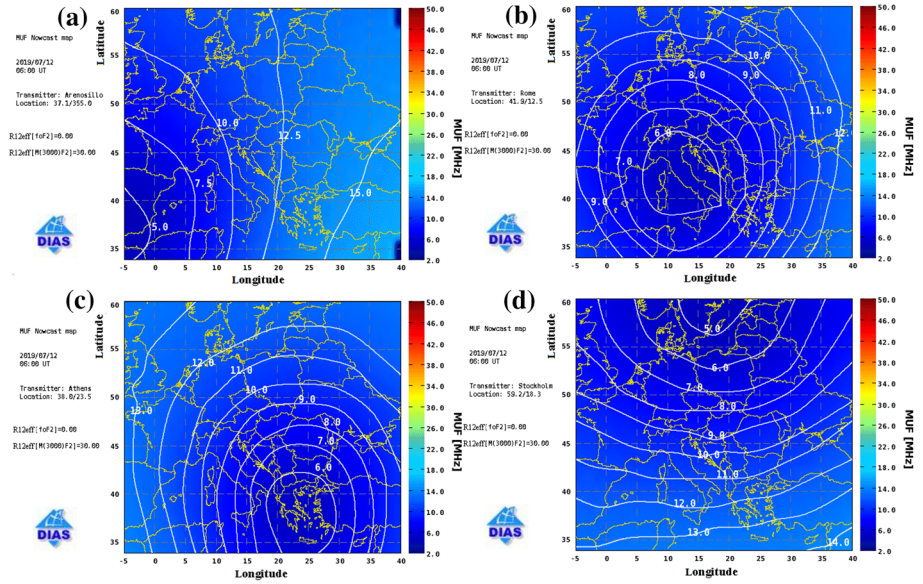

Fig. 17 MUF and skip distance nowcasting maps centred on **a** El Arenosillo, **b** Rome, **c** Athens, and **d** Stockholm on 12 July 2019 at 06:00 UT

- to pass from a high-latitude zone to a mid-latitude one a buffer zone (60° N–50° N) was considered. In this buffer zone, *fo*F2 predictions obtained from the CCIR model, using $R_{12\text{eff}}(foF2)_{\text{high}}$, and from the SIRMUP model, using $R_{12\text{eff}}(foF2)_{\text{mid}}$, were linearly interpolated giving a suitable weight according to the latitude (see Pietrella 2015 for details). $R_{12\text{eff}}(foF2)_{\text{mid}}$ is calculated on the basis of *fo*F2 autoscaled values from the mid-latitude European DIAS digisondes network.
- the SIRMUP procedure (Zolesi et al. 2004) is applied for the mid-latitude zone (34° N–60° N), using as input $R_{12\text{eff}}(foF2)_{\text{mid}}$.

Graphical procedures were then applied to represent the *fo*F2 maps extended in longitude from 10° W to 40° E and in latitude from 34° N to 80° N. Figure 18 shows an example of this kind of map obtained for $R_{12\text{eff}}(foF2)_{\text{high}} = R_{12\text{eff}}(foF2)_{\text{mid}} = -10$ on 12 July 2019 at 07:00 UT.

d. The IRI-SIRMUP-P (ISP) model provides a three-dimensional (3-D) real-time imaging of the ionosphere over the Mediterranean area. To accomplish this task the model first ingests *fo*F2 and *M*(3000)F2 autoscaled values from some ionospheric stations, and then assimilates also the corresponding observed electron density profiles (Pezzopane et al. 2011; Pietrella et al. 2016). The ISP model is another nowcasting tool where the SIRMUP method is employed as an intermediate step of a more complex procedure. The reliability of the ISP output has been described and discussed in detail in several papers (Pezzopane et al. 2011, 2013; Settimi et al. 2013, 2015; Pietrella et al. 2016). An example of the capability of the ISP procedure is given in Fig. 19, where a comparison between the electron density profiles extracted from the ISP 3-D matrix and those measured by ionosondes and modelled by the IRI model is shown. Another evidence of the good ISP performance can be appreciated in Fig. 20 showing a comparison between

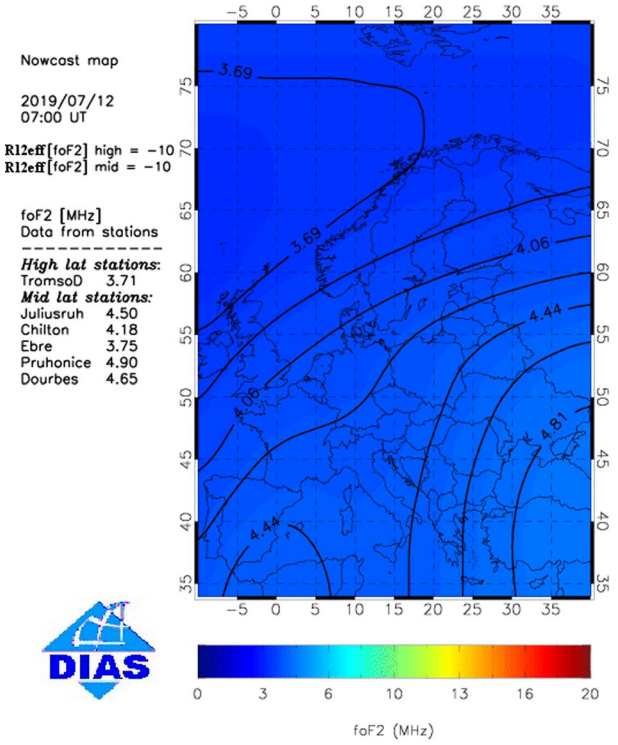

Fig. 18 Example of nowcasting map of *fo*F2 extended to high latitudes on 12 July 2019 at 07:00 UT. On the left side are listed the ionospheric stations involved in the calculation of $R_{12\text{eff}}(fo\text{F2})_{\text{high}}$ and $R_{12\text{eff}}(fo\text{F2})_{\text{mid}}$

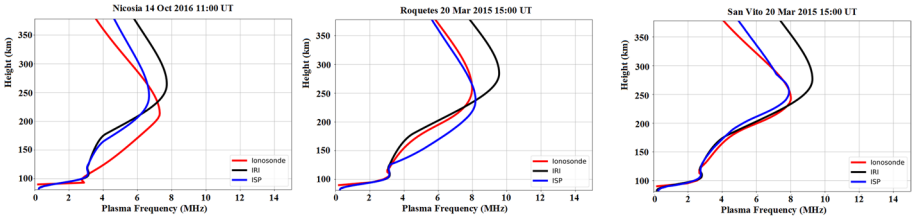

Fig. 19 Comparisons between electron density profiles measured respectively at (left) Nicosia, (middle), Roquetes (Ebre), and (right) San Vito and corresponding ISP and IRI ones

measured and synthesized ionograms. Synthesized ionograms are generated through the IONOspheric Ray Tracing (IONORT) tool developed by Azzarone et al. (2012) when ingesting IRI and ISP 3-D electron density representations (Pietrella et al. 2018).

e. A method to produce nowcasting maps of the MUF and skip distance isolines over Italy based on the SIRMUP model has been recently developed (Pietrella and Pezzopane 2020). In this case, the SIRM model is updated through the *fo*F2 and *M*(3000)F2 values autoscaled at the ionospheric stations of Rome and Gibilmanna. Two examples of these maps obtained combining the values of $R_{12\text{eff}}(fo\text{F2}) = -10$ and $R_{12\text{eff}}(M(3000)\text{F2}) = -70$, calculated on the basis of measurements autoscaled at Rome ($fo\text{F2} = 4.70$ MHz, $M(3000)\text{F2} = 3.23$) and Gibilmanna ($fo\text{F2} = 5.20$ MHz, $M(3000)\text{F2} = 3.40$) on 18 July 2018 at 16:00 UT, are given in Fig. 21.

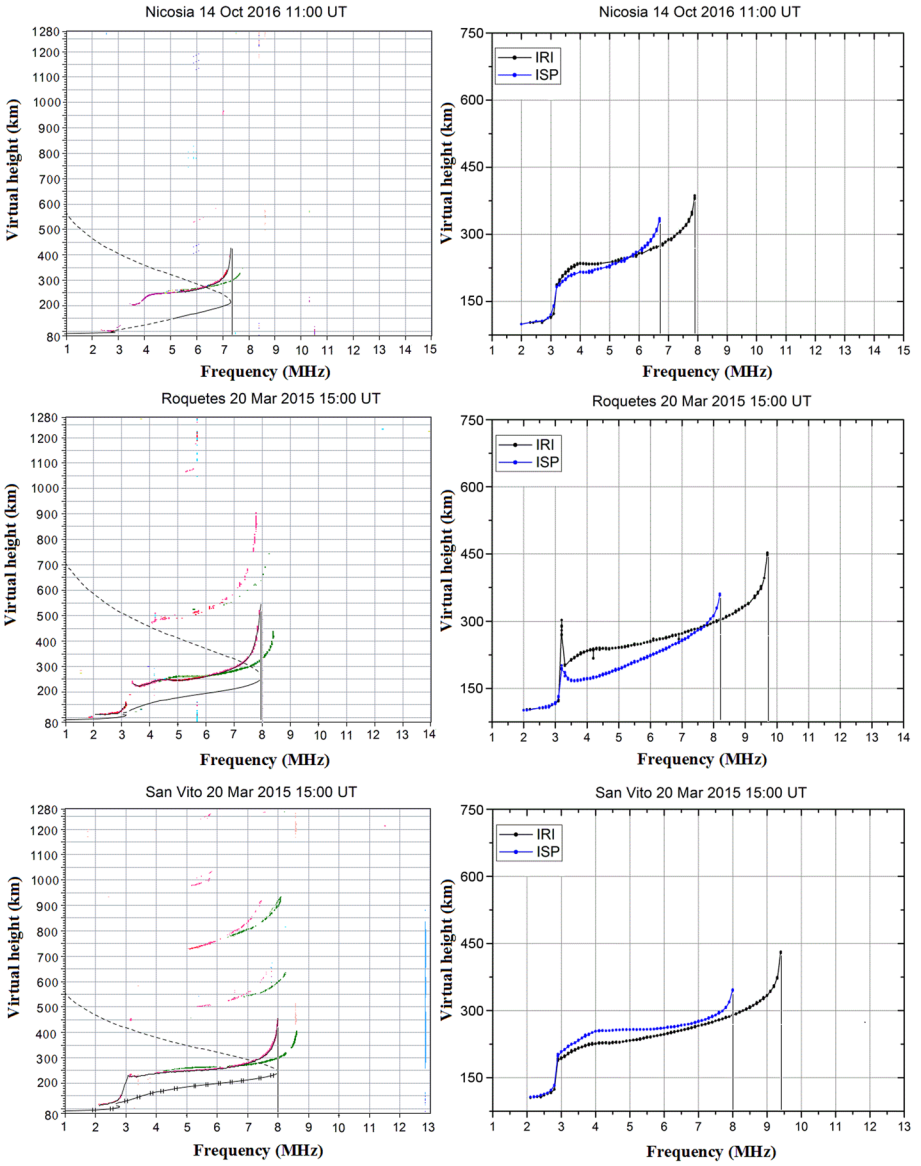

Fig. 20 (left) Measured ionograms and (right) corresponding synthetic quasi-vertical ionograms obtained through IONORT for (top row) Nicosia, (middle row) Roquetes (Ebre) and (bottom row) San Vito. Vertical lines highlight *fo*F2 values. On the right, blue and black ordinary traces are those synthesized respectively on the basis of the ISP and IRI model

5 Discussion and Future Developments

This paper is a review of the SIRM model, from the early stage of development to its present form. Moreover, some additional mathematical aspects of SIRM, never published so far, have been specifically addressed and described in detail.

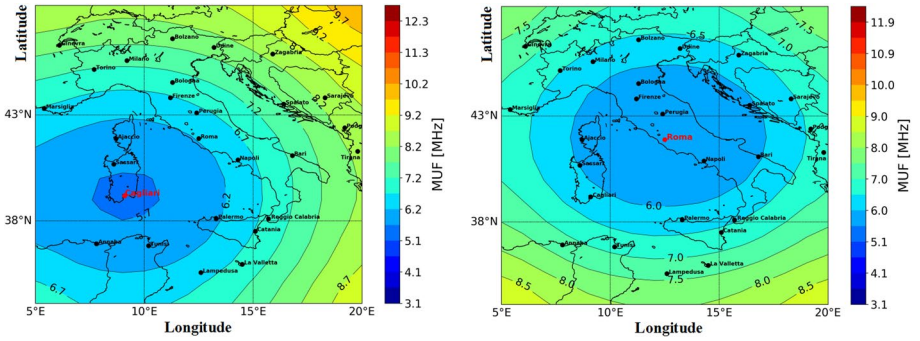

Fig. 21 MUF and corresponding skip distance nowcasting maps over Italy centred on (left) Cagliari, in western Italy, and (right) Rome, in central Italy, on 18 July 2018 at 16:00 UT

Although the improved SIRM and its updated version SIRMUP have been successfully employed in different applications during more than two decades, some weak points remain: (1) the assumption of a linear regression between the hourly monthly medians values of *fo*F2 and *M*(3000)F2 and the solar activity index R_{12}, which does not take properly into account saturation effects and hysteresis phenomena characterizing the ionospheric characteristics along the solar cycle; (2) the assumption of a linear fit between the Fourier coefficients (both in amplitude and phase) and R_{12}; (3) the absence of a dependence on longitude.

To eliminate these "weaknesses", a new version of the SIRM model, named SIRMpol, has been recently developed for the ionospheric station of Rome (Perna et al. 2017). Specifically, the numerical coefficients were recalculated and used to predict *fo*F2 over Rome according to the following three main steps: (a) a longer dataset of *fo*F2 values recorded at Rome; (b) second order polynomial regressions between *fo*F2 hourly monthly median values and R_{12}; (c) polynomial fits between Fourier coefficients and R_{12}. Notwithstanding the fact that the SIRMpol model still neglects the dependence on longitude, test results have shown that its output is better than the SIRM one, offering some useful guidelines to extend the improvement at a regional level.

Namely, taking into account a greater number of reference ionospheric stations spatially distributed in a homogeneous way, considerably enhanced historical datasets over each single reference station, and advanced numerical methods, a significant improvement of current SIRM and SIRMUP procedures could be expected over their validity area. Moreover, the accuracy of *fo*F2 and *M*(3000)F2 predictions could be further improved considering also the dependence on longitude. Obviously, the implementation of all these matters would imply a recalculation of numerical coefficients (for both *fo*F2 and *M*(3000)F2) over each reference station. However, when these steps are to be implemented, the introduction of the re-elaborated SIRM and SIRMUP in the current products offered by GIFINT, DIAS, SSA program, ESPAS and ISP will be worth the effort. Lastly and very importantly, for the first time the SIRM Fortran code is now downloadable for public usage at https://drive.google.com/file/d/1_tblhZBX2yEUPHDp_WINxyFBZoTPXIGa/view?usp=sharing

Acknowledgements The authors are grateful to both unknown reviewers for their helpful comments and suggestions that contributed to significantly improve the paper.

Appendix

Appendix 1.1: Phase Correction of the Fourier synthesis

A detailed description about how the phase of the Fourier synthesis has been corrected to consider the displacement of the reference ionospheric station from the central meridian of the time zone is here reported. In what follows R_{12} is the 12-month running mean of the monthly sunspot number R, m is the month of the year, n is the harmonic number, and $h^* = (1/15°)$ is a conversion factor to express longitude differences in hours or fraction of hours.

Let us hypothesize the case of ionospheric stations located respectively to west or east of the central meridian of whatever time zone (Fig. 22).

It is important to note that hourly time series of monthly median values of the generic ionospheric characteristic refer to the local standard time t_{CM} of the central meridian,

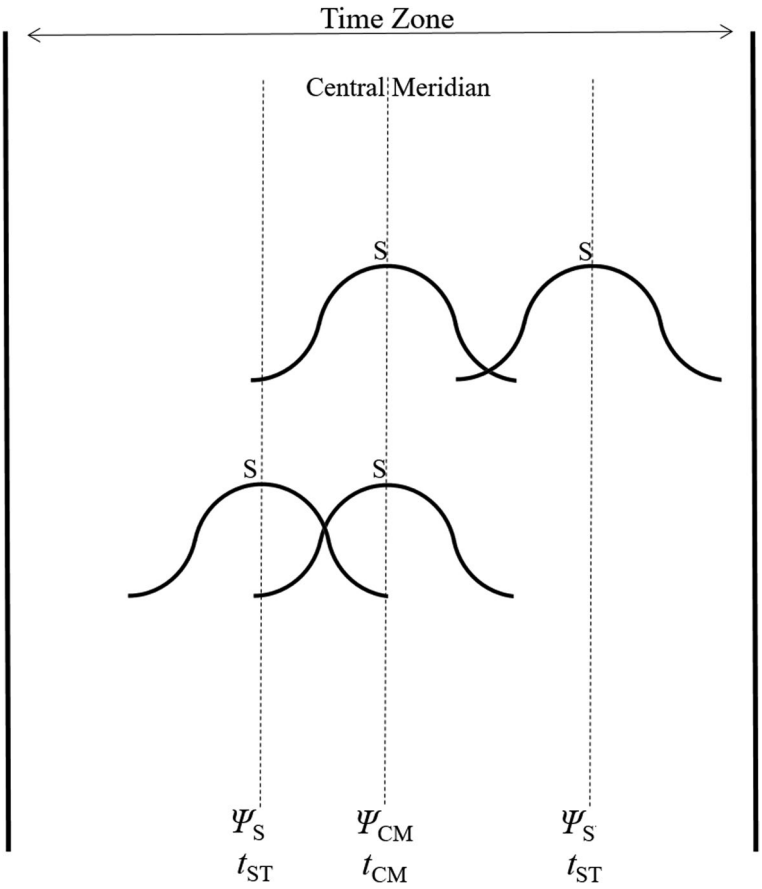

Fig. 22 Sketch showing the longitude Ψ_S of a station S, that can be located eastward or westward of the central meridian, and its corresponding solar time t_{ST}, the longitude Ψ_{CM} of the central meridian and its corresponding local standard time t_{CM}. The bell-shaped drawings represent the hourly time series of monthly median values of the generic ionospheric characteristic at longitudes Ψ_S and Ψ_{CM}

because measurements at S are recorded right at the time t_{CM}. Nevertheless, values are affected by the zenithal solar angle and this implies that time series must be referred to solar times t_{ST}. This will not imply a variation of values but only their translation in time with respect to the central meridian, meaning that Fourier coefficients of the amplitude remain unchanged. In the light of these considerations, we will show how to carry out the phase correction for a station positioned on both the west and east sides of the central meridian.

The diurnal variation of hourly monthly median values of the generic ionospheric characteristic (Ω) has a period $T=24$ h and, generalizing Eq. (8) for a station S, for a given month and R_{12}, at the central meridian it can be exactly represented by the following Fourier synthesis:

$$\Omega\left(t_{CM},R_{12},m\right)_S = A\left(\Psi_{CM},R_{12},m\right)_{S,0} + \sum_{n=1}^{12} A\left(\Psi_{CM},R_{12},m\right)_{S,n} \sin\left(\frac{2\pi n t_{CM}}{T} + Y\left(\Psi_{CM},R_{12},m\right)_{S,n}\right); \tag{10}$$

anyhow, to refer Ω to the solar time t_{ST} of the station S, (10) has to be corrected. At t_{ST} the time series is represented by the following Fourier synthesis:

$$\Omega\left(t_{ST},R_{12},m\right)_S = A\left(\Psi_S,R_{12},m\right)_{S,0} + \sum_{n=1}^{12} A\left(\Psi_S,R_{12},m\right)_{S,n} \sin\left(\frac{2\pi n t_{ST}}{T} + Y\left(\Psi_S,R_{12},m\right)_{S,n}\right); \tag{11}$$

in (10)–(11),Ψ_S andΨ_{CM} ranges in $(-180°;180]$.

The solar time t_{ST} is calculated through the mathematical function named floor, that gives the greatest integer that is less than or equal to its argument, as

$$t_{ST} = a - b \cdot \text{floor}(a/b); \tag{12}$$

specifically, in (12) $a=[t_{CM}+(\Psi_S-\Psi_{CM})h^*]$ and $b=T=24$ (number of hours in a day).

By using (12), independently of the station location (eastward or westward of the central meridian), t_{ST} is always within the range [0,24). For example, if the station is located at a longitude 30° eastward of the central meridian and $t_{CM}=0$, then $a=2$; by inserting $a=2$ and $b=24$ in (12), because floor(2/24)=0, it can be easily verified that $t_{ST}=2$. Likewise, if the station is located at a longitude 30° westward of the central meridian and $t_{CM}=0$, then $a=-2$; by inserting $a=-2$ and $b=24$ in (12), because floor(−2/24)=−1, it can be easily verified that $t_{ST}=22$.

From (10) and (11) it has to be

$$\Omega\left(t_{CM},R_{12},m\right)_S = \Omega\left(t_{ST},R_{12},m\right)_S; \tag{13}$$

(13) implies that

$$A\left(\Psi_{CM},R_{12},m\right)_{S,0} = A\left(\Psi_S,R_{12},m\right)_{S,0}, \tag{14}$$

$$A\left(\Psi_{CM},R_{12},m\right)_{S,n} = A\left(\Psi_S,R_{12},m\right)_{S,n}, \tag{15}$$

and

$$\sin\left(\frac{2\pi n t_{CM}}{T} + Y\left(\Psi_{CM},R_{12},m\right)_{S,n}\right) = \sin\left(\frac{2\pi n t_{ST}}{T} + Y\left(\Psi_S,R_{12},m\right)_{S,n}\right); \tag{16}$$

considering (12), the right side of (16) becomes

$$\sin\left\{\frac{2\pi n t_{\mathrm{CM}}}{T}+\frac{2\pi n}{T}\left[\Delta\Psi_{\mathrm{S,CM}}h^{*}-T\cdot\mathrm{floor}\left(\frac{t_{\mathrm{CM}}+\Delta\Psi_{\mathrm{S,CM}}h^{*}}{T}\right)\right]+Y\left(\Psi_{\mathrm{S}},R_{12},m\right)_{\mathrm{S},n}\right\},\tag{17}$$

where $\Delta\Psi_{\mathrm{S,CM}}=(\Psi_{\mathrm{S}}-\Psi_{\mathrm{CM}})$. From (16) and (17) it follows that

$$Y\left(\Psi_{\mathrm{S}},R_{12},m\right)_{\mathrm{S},n}=Y\left(\Psi_{\mathrm{CM}},R_{12},m\right)_{\mathrm{S},n}-\frac{2\pi n}{T}\left[\Delta\Psi_{\mathrm{S,CM}}h^{*}-T\cdot\mathrm{floor}\left(\frac{t_{\mathrm{CM}}+\Delta\Psi_{\mathrm{S,CM}}h^{*}}{T}\right)\right].\tag{18}$$

(18) shows the relationship between phases of (10) and (11), the former related to the central meridian, the latter related to the station meridian.

Appendix 1.2: The SIRM Algorithm

In this section the SIRM prediction algorithm will be described in detail indicating with Ω the ionospheric characteristic (*fo*F2 or *M*(3000)F2). Referring to Fig. 22, the regression analysis carried out month by month between hourly monthly median values of Ω and R_{12} provides, for each hour (h) and month (m), the coefficients $\alpha(h,m)_{\mathrm{S}}$ and $\beta(h,m)_{\mathrm{S}}$ for a definite station S. So, from the empirical law

$$\Omega_{\mathrm{S}}\left(h,m,R_{12}\right)=\alpha(h,m)_{\mathrm{S}}R_{12}+\beta(h,m)_{\mathrm{S}},\tag{19}$$

diurnal trends of hourly monthly median values are calculated for $R_{12}=0$ and $R_{12}=100$; the corresponding two time series can be represented through the Fourier synthesis as follows:

$$\Omega\left(t_{\mathrm{CM}},R_{12}=0,m\right)_{\mathrm{S}}=A\left(\Psi_{\mathrm{CM}},R_{12}=0,m\right)_{\mathrm{S},0}+\sum_{n=1}^{12}A\left(\Psi_{\mathrm{CM}},R_{12}=0,m\right)_{\mathrm{S},n}\sin\left(\frac{2\pi n t_{\mathrm{CM}}}{T}+Y\left(\Psi_{\mathrm{CM}},R_{12}=0,m\right)_{\mathrm{S},n}\right),\tag{20a}$$

$$\Omega\left(t_{\mathrm{CM}},R_{12}=100,m\right)_{\mathrm{S}}=A\left(\Psi_{\mathrm{CM}},R_{12}=100,m\right)_{\mathrm{S},0}+\sum_{n=1}^{12}A\left(\Psi_{\mathrm{CM}},R_{12}=100,m\right)_{\mathrm{S},n}\sin\left(\frac{2\pi n t_{\mathrm{CM}}}{T}+Y\left(\Psi_{\mathrm{CM}},R_{12}=100,m\right)_{\mathrm{S},n}\right),\tag{20b}$$

being $T=24$ h.

(20a–20b) reconstruct exactly the time series $\Omega(t_{\mathrm{CM}},R_{12},m)_{\mathrm{S}}$ for $R_{12}=0$ and $R_{12}=100$. It is important to point out that time series provided by (20a–20b) are referred to t_{CM}, because measurements at S are recorded at the time t_{CM}. Nevertheless, as highlighted in the Appendix 1.1, measurements are somehow affected by the zenithal solar angle, which means that (20a–20b) must be rewritten as a function of the solar times t_{ST} of S. Therefore, a phase correction of the Fourier synthesis is needed, while coefficients of the amplitude remain unchanged. To this regard, exploiting (14) and (15) obtained in the Appendix 1.1, (20a–20b) become

$$\Omega\left(t_{\mathrm{ST}}, R_{12}=0, m\right)_{\mathrm{S}} = A\left(\Psi_S, R_{12}=0, m\right)_{\mathrm{S},0} + \sum_{n=1}^{12} A\left(\Psi_S, R_{12}=0, m\right)_{\mathrm{S},n} \sin\left(\frac{2\pi n t_{\mathrm{ST}}}{T} + Y\left(\Psi_{\mathrm{S}}, R_{12}=0, m\right)_{\mathrm{S},n}\right), \tag{21a}$$

$$\Omega\left(t_{\mathrm{ST}}, R_{12}=100, m\right)_{\mathrm{S}} = A\left(\Psi_S, R_{12}=100, m\right)_{\mathrm{S},0} + \sum_{n=1}^{12} A\left(\Psi_S, R_{12}=100, m\right)_{\mathrm{S},n} \sin\left(\frac{2\pi n t_{\mathrm{ST}}}{T} + Y\left(\Psi_{\mathrm{S}}, R_{12}=100, m\right)_{\mathrm{S},n}\right), \tag{21b}$$

where the phases in (21a–21b) are calculated by (18).

(21a–21b) refer to solar times and represent the algorithms for the prediction of hourly monthly median values, respectively, over S for $R_{12}=0$ and $R_{12}=100$; to get values of Ω for any value of R_{12}, a linear trend between Fourier coefficients and R_{12} is supposed. Specifically, straight lines passing through points

$$\left(R_{12}=0; A\left(\Psi_{\mathrm{S}}, R_{12}=0, m\right)_{\mathrm{S},0}\right) \text{and} \left(R_{12}=100; A\left(\Psi_{\mathrm{S}}, R_{12}=100, m\right)_{\mathrm{S},0}\right), \tag{22a}$$

$$\left(R_{12}=0; A\left(\Psi_{\mathrm{S}}, R_{12}=0, m\right)_{\mathrm{S},n}\right) \text{and} \left(R_{12}=100; A\left(\Psi_{\mathrm{S}}, R_{12}=100, m\right)_{\mathrm{S},n}\right), \tag{22b}$$

$$\left(R_{12}=0; Y\left(\Psi_{\mathrm{S}}, R_{12}=0, m\right)_{\mathrm{S},n}\right) \text{and} \left(R_{12}=100; Y\left(\Psi_{\mathrm{S}}, R_{12}=100, m\right)_{\mathrm{S},n}\right), \tag{22c}$$

are considered; (22a) provides the angular coefficient $a(m)_{\mathrm{S},0}$ and intercept $b(m)_{\mathrm{S},0}$; (22b) provides 12 angular coefficients $a(m)_{\mathrm{S},n}$ and 12 intercepts $b(m)_{\mathrm{S},n}$; (22c) provides 12 angular coefficients $c(m)_{\mathrm{S},n}$ and 12 intercepts $d(m)_{\mathrm{S},n}$.

These angular coefficients and intercepts are then used to calculate amplitudes and corresponding phases of each harmonic, for a generic value of R_{12}, through the following empirical laws

$$A\left(\Psi_{\mathrm{S}}, R_{12}, m\right)_{\mathrm{S},0} = a(m)_{\mathrm{S},0} R_{12} + b(m)_{\mathrm{S},0}, \tag{23a}$$

$$A\left(\Psi_{\mathrm{S}}, R_{12}, m\right)_{\mathrm{S},n} = a(m)_{\mathrm{S},n} R_{12} + b(m)_{\mathrm{S},n}, \tag{23b}$$

$$Y\left(\Psi_{\mathrm{S}}, R_{12}, m\right)_{\mathrm{S},n} = c(m)_{\mathrm{S},n} R_{12} + d(m)_{\mathrm{S},n}. \tag{23c}$$

So, considering (23a–23c), the Fourier synthesis

$$\Omega\left(t_{\mathrm{ST}}, R_{12}, m\right)_{\mathrm{S}} = \left(a(m)_{\mathrm{S},0} R_{12} + b(m)_{\mathrm{S},0}\right) + \sum_{n=1}^{12} \left(a(m)_{\mathrm{S},n} R_{12} + b(m)_{\mathrm{S},n}\right) \sin\left[\frac{2\pi n t_{\mathrm{ST}}}{T} + \left(c(m)_{\mathrm{S},n} R_{12} + d(m)_{\mathrm{S},n}\right)\right] \tag{24}$$

can predict the hourly monthly median values over S for whatever value of R_{12}. Relation (24) represents a local prediction model that can be applied only over S. To develop a regional model it is necessary to consider a definite number of ionospheric stations that have regularly operated for a relatively long period inside a given area, which is the validity

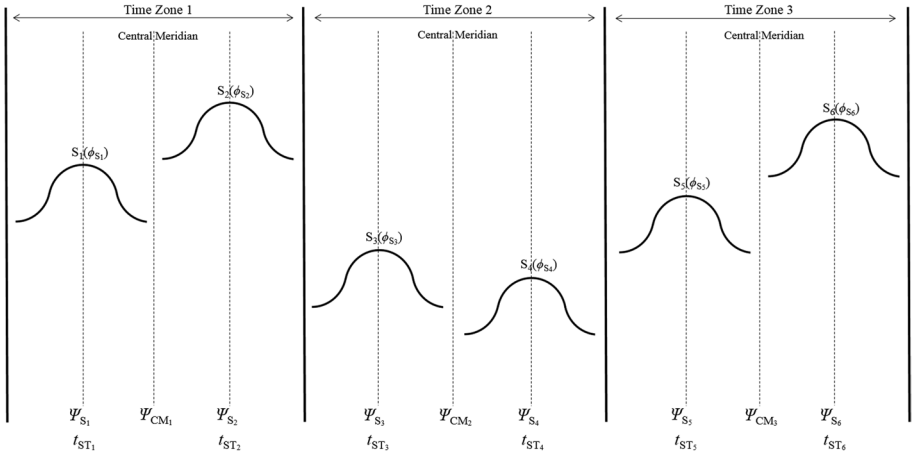

Fig. 23 Six ionospheric stations S_i (with $i=1,\ldots,6$) distributed in three different time zones: three located to west and three to east of the corresponding central meridian, whose longitude is Ψ_{CMj} (with $j=1,\ldots,3$).Ψ_{Si}, ϕ_{Si} and t_{STi} (with $i=1,\ldots,6$) are corresponding longitudes, latitudes and solar times

area of the model. For simplicity, let us consider only six ionospheric stations distributed as in Fig. 23.

According to (24) we can write

$$\begin{aligned}\Omega\left(t_{\mathrm{ST_i}}, R_{12}, m\right)_{\mathrm{S}_i} &= \left(a(m)_{\mathrm{S}_i,0} R_{12} + b(m)_{\mathrm{S}_i,0}\right) \\ &+ \sum_{n=1}^{12} \left(a(m)_{\mathrm{S}_i,n} R_{12} + b(m)_{\mathrm{S}_i,n}\right) \sin\left[\frac{2\pi n t_{\mathrm{ST_i}}}{T} + \left(c(m)_{\mathrm{S}_i,n} R_{12} + d(m)_{\mathrm{S}_i,n}\right)\right],\end{aligned} \tag{25}$$

with $i=1,\ldots, 6$.

Assuming that ionospheric stations are distributed in a relatively restricted area, we can guess that values depend more on latitude than on longitude. Moreover, once the diurnal trends refer to solar times of ionospheric stations, time series are in "phase", and the dependence on the latitude can be assessed by making a linear regression between amplitude and phase coefficients of the Fourier synthesis against latitudes of the ionospheric stations. Therefore, in the considered example, a linear trend between coefficients of (25) and the latitude of ionospheric stations is supposed and linear regressions (LR_s) are made considering the following datasets of points:

$$\mathrm{LR}_1 \rightarrow \left(\phi_{\mathrm{S}_1}; a(m)_{\mathrm{S}_1,0}\right), \left(\phi_{\mathrm{S}_2}; a(m)_{\mathrm{S}_2,0}\right), \left(\phi_{\mathrm{S}_3}; a(m)_{\mathrm{S}_3,0}\right), \left(\phi_{\mathrm{S}_4}; a(m)_{\mathrm{S}_4,0}\right), \left(\phi_{\mathrm{S}_5}; a(m)_{\mathrm{S}_5,0}\right), \left(\phi_{\mathrm{S}_6}; a(m)_{\mathrm{S}_6,0}\right); \tag{26a}$$

$$\mathrm{LR}_2 \rightarrow \left(\phi_{\mathrm{S}_1}; b(m)_{\mathrm{S}_1,0}\right), \left(\phi_{\mathrm{S}_2}; b(m)_{\mathrm{S}_2,0}\right), \left(\phi_{\mathrm{S}_3}; b(m)_{\mathrm{S}_3,0}\right), \left(\phi_{\mathrm{S}_4}; b(m)_{\mathrm{S}_4,0}\right), \left(\phi_{\mathrm{S}_5}; b(m)_{\mathrm{S}_5,0}\right), \left(\phi_{\mathrm{S}_6}; b(m)_{\mathrm{S}_6,0}\right); \tag{26b}$$

$$\mathrm{LR}_3 \rightarrow \left(\phi_{\mathrm{S}_1}; a(m)_{\mathrm{S}_1,n}\right), \left(\phi_{\mathrm{S}_2}; a(m)_{\mathrm{S}_2,n}\right), \left(\phi_{\mathrm{S}_3}; a(m)_{\mathrm{S}_3,n}\right), \left(\phi_{\mathrm{S}_4}; a(m)_{\mathrm{S}_4,n}\right), \left(\phi_{\mathrm{S}_5}; a(m)_{\mathrm{S}_5,n}\right), \left(\phi_{\mathrm{S}_6}; a(m)_{\mathrm{S}_6,n}\right); \tag{26c}$$

$$\mathrm{LR}_4 \rightarrow \left(\phi_{\mathrm{S}_1}; b(m)_{\mathrm{S}_1,n}\right), \left(\phi_{\mathrm{S}_2}; b(m)_{\mathrm{S}_2,n}\right), \left(\phi_{\mathrm{S}_3}; b(m)_{\mathrm{S}_3,n}\right), \left(\phi_{\mathrm{S}_4}; b(m)_{\mathrm{S}_4,n}\right), \left(\phi_{\mathrm{S}_5}; b(m)_{\mathrm{S}_5,n}\right), \left(\phi_{\mathrm{S}_6}; b(m)_{\mathrm{S}_6,n}\right); \tag{26d}$$

$$\mathrm{LR}_5 \rightarrow \left(\phi_{\mathrm{S}_1};c(m)_{\mathrm{S}_1,n}\right),\left(\phi_{\mathrm{S}_2};c(m)_{\mathrm{S}_2,n}\right),\left(\phi_{\mathrm{S}_3};c(m)_{\mathrm{S}_3,n}\right),\left(\phi_{\mathrm{S}_4};c(m)_{\mathrm{S}_4,n}\right),\left(\phi_{\mathrm{S}_5};c(m)_{\mathrm{S}_5,n}\right),\left(\phi_{\mathrm{S}_6};c(m)_{\mathrm{S}_6,n}\right); \tag{26e}$$

$$\mathrm{LR}_6 \rightarrow \left(\phi_{\mathrm{S}_1};d(m)_{\mathrm{S}_1,n}\right),\left(\phi_{\mathrm{S}_2};d(m)_{\mathrm{S}_2,n}\right),\left(\phi_{\mathrm{S}_3};d(m)_{\mathrm{S}_3,n}\right),\left(\phi_{\mathrm{S}_4};d(m)_{\mathrm{S}_4,n}\right),\left(\phi_{\mathrm{S}_5};d(m)_{\mathrm{S}_5,n}\right),\left(\phi_{\mathrm{S}_6};d(m)_{\mathrm{S}_6,n}\right). \tag{26f}$$

LR_1 provides the angular coefficient $a(m)_0^1$ and intercept $a(m)_0^2$; LR_2 provides the angular coefficient $b(m)_0^1$ and intercept $b(m)_0^2$; LR_3 provides the angular coefficient $a(m)_n^1$ and intercept $a(m)_n^2$; LR_4 provides the angular coefficient $b(m)_n^1$ and intercept $b(m)_n^2$; LR_5 provides the angular coefficient $c(m)_n^1$ and intercept $c(m)_n^2$; LR_6 provides the angular coefficient $d(m)_n^1$ and intercept $d(m)_n^2$. Accordingly, the following empirical laws are obtained

$$a(m)_0 = a(m)_0^1\phi + a(m)_0^2, \tag{27a}$$

$$b(m)_0 = b(m)_0^1\phi + b(m)_0^2, \tag{27b}$$

$$a(m)_n = a(m)_n^1\phi + a(m)_n^2, \tag{27c}$$

$$b(m)_n = b(m)_n^1\phi + b(m)_n^2, \tag{27d}$$

$$c(m)_n = c(m)_n^1\phi + c(m)_n^2, \tag{27e}$$

$$d(m)_n = d(m)_n^1\phi + d(m)_n^2. \tag{27f}$$

So, for a given month, (27a–27f) show how Fourier coefficients change as the latitude varies; specifically, there are four coefficients ($a(m)_0^1$; $a(m)_0^2$; $b(m)_0^1$; $b(m)_0^2$) for the average term and eight coefficients ($a(m)_n^1$; $a(m)_n^2$; $b(m)_n^1$; $b(m)_n^2$; $c(m)_n^1$; $c(m)_n^2$; $d(m)_n^1$; $d(m)_n^2$)

Table 4 Numerical coefficients used by SIRM to predict *fo*F2 in January

	$a(1)_0^1$	$a(1)_0^2$	$b(1)_0^1$	$b(1)_0^2$				
	−0.830	268.270	−0.615	62.401				
n	$a(1)_n^1$	$a(1)_n^2$	$b(1)_n^1$	$b(1)_n^2$	$c(1)_n^1$	$c(1)_n^2$	$d(1)_n^1$	$d(1)_n^2$
1	1.000	174.19	−0.188	20.775	0.020	−0.001	−2.180	4.390
2	2.180	−66.09	0.041	5.416	−0.160	−0.010	7.820	1.291
3	−0.930	82.55	−0.019	2.584	−0.060	−0.070	4.190	8.855
4	−0.070	17.94	−0.080	6.255	−0.520	−0.016	21.850	3.971
5	−0.320	26.08	0.007	0.410	1.580	−0.005	−86.030	2.502
6	0.210	−6.52	−0.019	1.957	0.010	0.037	1.950	1.844
7	0.090	−1.75	−0.022	1.940	0.220	−0.092	−7.060	7.010
8	0.080	−1.71	−0.015	1.345	0.430	0.056	−35.140	0.803
9	0.030	−0.23	−0.011	1.218	0.280	−0.121	−11.630	10.316
10	−0.010	1.62	0.003	0.243	−0.850	−0.009	39.840	3.170
11	0.040	−1.34	−0.004	0.602	−0.560	0.022	30.760	1.279
12	0.000	0.32	0.004	0.149	0.430	−0.107	−24.020	9.132

for each of the twelve harmonics, thus obtaining for a given month a total number of 100 coefficients.

Thanks to (27a–27f), (25) can be then generalized in the context of a regional model so that the prediction algorithm can be synthetically written as follows

$$\Omega(t_{ST},\phi,R_{12},m)=\left(a(m)_0^1\phi+a(m)_0^2\right)R_{12}+b(m)_0^1\phi+b(m)_0^2 + \sum_{n=1}^{12}\left[\left(a(m)_n^1\phi+a(m)_n^2\right)R_{12}+b(m)_n^1\phi+b(m)_n^2\right]\sin\left\{\frac{2\pi n t_{ST}}{T}+\left[\left(c(m)_n^1\phi+c(m)_n^2\right)R_{12}+d(m)_n^1\phi+d(m)_n^2\right]\right\}. \tag{28}$$

It is worth mentioning once again that in (28) coefficients depend on the month, which means that SIRM is represented by 12·100 = 1200 coefficients. For example, Table 4 shows the 100 numerical coefficients used by SIRM to predict *fo*F2 in January.

Let us focus now on the issue about the dependence on longitude. The prediction algorithm (28), referred to the Greenwich prime meridian, for which t_{ST} ($\Psi_{CM}=0°$) = t_{UT}, is

$$\Omega(t_{UT},\phi,R_{12},m)=\left(a(m)_0^1\phi+a(m)_0^2\right)R_{12}+b(m)_0^1\phi+b(m)_0^2 + \sum_{n=1}^{12}\left[\left(a(m)_n^1\phi+a(m)_n^2\right)R_{12}+b(m)_n^1\phi+b(m)_n^2\right]\sin\left\{\frac{2\pi n t_{UT}}{T}+\left[\left(c(m)_n^1\phi+c(m)_n^2\right)R_{12}+d(m)_n^1\phi+d(m)_n^2\right]\right\}. \tag{29}$$

If in (29) we set ϕ = cost, values of $\Omega(t_{UT},\phi,R_{12},m)$ are modulated at various hours essentially by the amplitude coefficients; this means that time series obtained at different longitudes, varying in (29) t_{UT} from 00:00 to 23:00, will be always the same not only for the shape but also for the positioning with respect to the corresponding prime meridian, which is unacceptable.

To overcome this issue, over a restricted validity area, the dependence on longitude is considered in the following way: $\Omega(t_{UT},\phi,R_{12},m)$ values are first referred to the prime meridian ($\Psi=0°$) using (29) and then translated in time, $t_{UT}\rightarrow t_{UT}-\Psi h^*$, being Ψ the longitude of the generic meridian, namely

$$\Omega(t_{UT},\phi,R_{12},m)=\left(a(m)_0^1\phi+a(m)_0^2\right)R_{12}+b(m)_0^1\phi+b(m)_0^2 + \sum_{n=1}^{12}\left[\left(a(m)_n^1\phi+a(m)_n^2\right)R_{12}+b(m)_n^1\phi+b(m)_n^2\right]\sin\left\{\frac{2\pi n\left(t_{UT}-\psi h^*\right)}{T} + \left[\left(c(m)_n^1\phi+c(m)_n^2\right)R_{12}+d(m)_n^1\phi+d(m)_n^2\right]\right\}, \tag{30}$$

so as to refer them to times depending on the meridian under consideration.

To clarify better how the algorithm (30) works, it is convenient to make a numerical example considering *fo*F2 time series reported in Table 5 obtained by applying the SIRM model for $\phi=40°$, $R_{12}=100$, and $m=1$ (which means that numerical coefficients of Table 4 have been used) at longitudes $\Psi=+15°$ and $\Psi=+30°$.

Let us indicate with S_{PM} the *fo*F2 time series at the prime meridian ($\Psi=0°$) (first column of Table 5). If we want to refer S_{PM} at the various meridians, it has to be moved opportunely according to the longitude. If the meridian at $\Psi=+15°$ is considered then $t_{UT}\rightarrow t_{UT}+1$ h; this means that if for example (29) provides a value of S_{PM} at $t_{UT}=12{:}00$ equal to 9.3 MHz, the same value is obtained through (30) at $\Psi=+15°$ at $t_{UT}=11{:}00$.

Therefore, S_{PM} will result translated in time one hour backward (second column of Table 5). If instead the meridian at $\Psi=+30°$ is considered then $t_{UT}\rightarrow t_{UT}+2$ h; this means

Table 5 *fo*F2 (MHz) time series provided in UT by the SIRM model for $R_{12}=100$, $m=1$ and $\phi=+40°$ at (first column) longitude $\Psi=0°$, (second column) $\Psi=+15°$, and (third column) $\Psi=+30°$

UT/*fo*F2 ($\Psi=0°$)	UT/*fo*F2 ($\Psi=+15°$)	UT/*fo*F2 ($\Psi=+30°$)
00:00/3.7	00:00/3.9	00:00/3.9
01:00/3.9	01:00/3.9	01:00/3.4
02:00/3.9	02:00/3.4	02:00/2.9
03:00/3.4	03:00/2.9	03:00/3.5
04:00/2.9	04:00/3.5	04:00/3.6
05:00/3.5	05:00/3.6	05:00/4.6
06:00/3.6	06:00/4.6	06:00/7.3
07:00/4.6	07:00/7.3	07:00/9.0
08:00/7.3	08:00/9.0	08:00/10.1
09:00/9.0	09:00/10.1	09:00/9.9
10:00/10.1	10:00/9.9	10:00/9.3
11:00/9.9	11:00/9.3	11:00/9.3
12:00/9.3	**12:00/9.3**	**12:00/9.9**
13:00/9.3	13:00/9.9	13:00/9.6
14:00/9.9	14:00/9.6	14:00/8.7
15:00/9.6	15:00/8.7	15:00/7.2
16:00/8.7	16:00/7.2	16:00/6.3
17:00/7.2	17:00/6.3	17:00/5.1
18:00/6.3	18:00/5.1	18:00/4.4
19:00/5.1	19:00/4.4	19:00/4.0
20:00/4.4	20:00/4.0	20:00/4.0
21:00/4.0	21:00/4.0	21:00/3.6
22:00/4.0	22:00/3.6	22:00/3.7
23:00/3.6	23:00/3.7	23:00/3.9

that if for example (29) provides a value of S_{PM} at $t_{UT}=08:00$ equal to 7.3 MHz, the same value is obtained through (30) at $\Psi=+30°$ at $t_{UT}=06:00$. In this case S_{PM} will result translated in time 2 h backward (third column of Table 5). Similar considerations hold in case of negative longitudes. It is worth highlighting that in this way, to a first approximation, and for a narrow area in longitude, the dependence on longitude is well represented. This is testified by Table 5 showing for example that values of *fo*F2 at 05:00 UT (i.e. *fo*F2 ($\Psi=30°$) = 4.6 MHz > *fo*F2 ($\Psi=15°$) = 3.6 MHz >, *fo*F2 ($\Psi=0°$) = 3.5 MHz) are consistent with the passage of the solar terminator at sunrise, while values of *fo*F2 at 18:00 UT (i.e. *fo*F2 ($\Psi=30°$) = 4.4 MHz < *fo*F2 ($\Psi=15°$) = 5.1 MHz < *fo*F2 ($\Psi=0°$) = 6.3 MHz) are consistent with the passage of the solar terminator at sunset.

From this procedure is then possible to get *fo*F2 maps in UT. Let us observe for example that, in the specific case of the bold row of Table 5, values of *fo*F2 at longitudes $\Psi=0°$ (9.3 MHz), $\Psi=+15°$ (9.3 MHz), and $\Psi=+30°$ (9.9 MHz), at latitude $\phi=+40°$, are all referred to 12:00 UT. This means that fixing the value of the latitude, the longitude can be varied with a one degree spatial resolution in order to get corresponding *fo*F2 values from (30). This procedure repeated varying also the latitude with a one degree spatial resolution allows to ultimately get a $1°\times1°$ grid of *fo*F2 values evenly spaced in longitude and latitude which are all referred to the same UT. The grid is then processed through a graphical tool to obtain a *fo*F2 map in UT over the area under consideration.

References

Azzarone A, Bianchi C, Pezzopane M, Pietrella M, Scotto C, Settimi A (2012) IONORT: a windows software tool to calculate the HF ray tracing in the ionosphere. Comput Geosci 42:57–63. https://doi.org/10.1016/j.cageo.2012.02.008

Belehaki A, Cander LR, Zolesi B, Bremer J, Juren C, Stanislawska I, Dialetis D, Hatzopoulos M (2005) DIAS project: the establishment of a European digital upper atmosphere server. J Atmos Solar Terr Phys 67(12):1092–1099. https://doi.org/10.1016/j.jastp.2005.02.021

Belehaki A, Cander LR, Zolesi B, Bremer J, Juren C, Stanislawska I, Dialetis D, Hatzopoulos M (2007) Ionospheric specification and forecasting based on observations from European ionosondes participating in DIAS project. Acta Geophys 55(3):398–409. https://doi.org/10.2478/s11600-007-0010-x

Belehaki A, Tsagouri I, Kutiev I, Marinov P, Zolesi B, Pietrella M, Themelis K, Elias P, Tziotziou K (2015) The European Ionosonde Service: nowcasting and forecasting ionospheric conditions over Europe for the ESA Space Situational Awareness services. J Space Weather Space Clim 5:A25. https://doi.org/10.1051/swsc/2015026

Belehaki A, James S, Hapgood M, Ventouras S, Galkin I, Lembesis A, Tsagouri I, Charisi A, Spogli L, Berdermann J, Haggstrom J (2016) The ESPAS consortium. The ESPAS e-infrastructure: access to data from near-Earth space. Adv Space Res 58:1177–1200. https://doi.org/10.1016/j.asr.2016.06.014

Bilitza D (1986) International reference ionosphere: recent developments. Radio Sci 21:343–346. https://doi.org/10.1029/RS021i003p00343

Bilitza D (1995) Including auroral boundaries in the IRI model. Adv Space Res 16(1):13–16. https://doi.org/10.1016/0273-1177(95)00093-T

Bilitza D (1997) International reference ionosphere—status 1995/96. Adv Space Res 20(9):1751–1754

Bilitza D (2001) International reference ionosphere 2000. Radio Sci 36:261–275. https://doi.org/10.1029/2000RS002432

Bilitza D (2018) IRI the International Standard for the Ionosphere. Adv Radio Sci 16:1–11. https://doi.org/10.5194/ars-16-1-2018

Bilitza D, Reinisch BW (2008) International reference ionosphere 2007: improvements and new parameters. Adv Space Res 42(7):599–609. https://doi.org/10.1016/j.asr.2007.07.048

Bilitza D, Rawer K, Bossy L, Kutiev I, Oyama KI, Leitinger R, Kazimirovsky E (1990) International reference ionosphere 1990. NSSDC 90-22, Greenbelt, Maryl., vol 53, p 160. http://dx.doi.org/10.1017/CBO9781107415324.004

Bilitza D, Altadill D, Zhang Y, Mertens C, Truhlik V, Richards P, McKinnell LA, Reinisch B (2014) The international reference ionosphere 2012—a model of international collaboration. J Space Weather Space Clim 4:A07. https://doi.org/10.1051/swsc/2014004

Bilitza D, Altadill D, Truhlik V, Shubin V, Galkin I, Reinisch B, Huang X (2017) International reference ionosphere 2016: from ionospheric climate to real-time weather predictions. Space Weather 15(2):418–429. https://doi.org/10.1002/2016SW001593

Bradley PA (1995) PRIME (Prediction and Retrospective Ionospheric Modelling over Europe), COST Action 238 final report, Comm. of the Eur. Communities, Brussels

Bradley PA, Cander LR, Dick M, Jodogne JC, Kouris SS, Leitinger R, Singer W, Xenos TD, Zolesi B (1994) The December 1993 new mapping meeting. In: Numerical mapping and modelling and their applications to PRIME, proceedings of the PRIME COST238 Workshop. Eindhoven Univ. of Technol, Eindhoven, Netherlands, pp 169–179

Cander LjR (2019) Ionospheric space weather. Springer Geophysics, Springer Nature Switzerland AG. https://doi.org/10.1007/978-3-319-99331-7

Cander LR, Milosavljevic MM, Stankovic SS, Tomasevic S (1998) Ionospheric forecasting technique by artificial neural network. Electron Lett 34(16):1573–1574

COST 251 VI Ionospheric Database on CD-ROM, Version 3, May 1999, Radio Communication Research Unit, Rutherford and Appleton Laboratory

De Franceschi G, De Santis A (1994) PASHA: regional long-term predictions of ionospheric parameters by ASHA. Ann Geophys. https://doi.org/10.4401/ag-4228

Dvinskikh NI (1988) Expansion of ionospheric characteristics fields in empirical orthogonal functions. Adv Space Res 8(4):179–187. https://doi.org/10.1016/0273-1177(88)90238-4

Galkin IA, Reinisch BW (2008) The new ARTIST 5 for all digisondes, in ionosonde network advisory group bulletin. In: IPS Radio and Space Serv., Surry Hills, N.S.W., Australia, vol 69, pp 1–8. http://www.ips.gov.au/IPSHosted/INAG/web-69/2008/artist5-inag.pdf. Accessed 2 July 2020

Hanbaba R (1999) Improved quality of services in telecommunication systems planning and operation, Action 251, final report. Space Research Center, Warsaw

Hochegger G, Nava B, Radicella S, Leitinger R (2000) A family of ionospheric models for different uses. Phys Chem Earth Part C Sol Terr Planet Sci 25(4):307–310. https://doi.org/10.1016/S1464-1917(00)00022-2

Houminer Z, Bennett JA, Dyson PL (1993) Real-time ionospheric model updating. J Electr Electr Eng 13(2):99–104

Jones WB, Gallet RM (1962) Representation of Diurnal and geographic variations of ionospheric data by numerical methods. Telecommun J 29(5):129–149

Jones WB, Gallet RM (1965) Representation of diurnal and geographic variations of ionospheric data by numerical methods II, control of instability. Telecommun J 32(1):18–28

Karpachev AT (2019) Variations in the winter troughs' position with local time, longitude, and solar activity in the Northern and Southern hemispheres. J Geophys Res 124(10):8039–8055. https://doi.org/10.1029/2019JA026631

Karpachev AT, Klimenko MV, Klimenko VV, Pustovalova LV (2016) Empirical model of the main ionospheric trough for nighttime winter conditions. J Atmos Sol Terr Phys 146:149–159. https://doi.org/10.1016/j.jastp.2016.05.008

Karpachev AT, Klimenko MV, Klimenko VV (2018) Longitudinal variations in the ionospheric trough position. Adv Space Res 63(2):950–966. https://doi.org/10.1016/j.asr.2018.09.038

Kouris SS, Alberca LF, Apostolov EM, Hanbaba R, Xenos TD, Zolesi B (1993) Proposals for the solar-cycle variations of foF2, II, in PRIME studies with emphasis on TEC and topside modelling, proceedings of the PRIME COST 238 workshop, pp 89–90, Wissenschaftlicher Bericht 2, part I, Karl-Franzens Univ., Graz, Austria

Lockwood M (1983) A simple M factor algorithm for improved estimation of the basic maximum frequency of radio waves reflected from the ionospheric F region. Proc IEE 130F:296–302

Mikhailov AV, Perrone L (2014) A method for foF2 short-term (1–24 h) forecast using both historical and real-time foF2 observations over European stations: EUROMAP model. Radio Sci 49:253–270. https://doi.org/10.1002/2014RS005373

Mikhailov AV, Mikhailov VV, Skoblin MG (1996) Monthly median foF2 and M(3000)F2 ionospheric model over Europe. Ann Geophys IT 39(4):791–805

Muhtarov P, Kutiev I (1999) Autocorrelation method for temporal interpolation and short-term prediction of ionospheric data. Radio Sci 34(2):459–464. https://doi.org/10.1029/1998RS900020

Nava B, Coisson P, Radicella SM (2008) A new version of the NeQuick ionosphere electron density model. J Atmos Solar Terr Phys. https://doi.org/10.1016/j.jastp.2008.01.015

Oyeyemi EO, Poole AWV, McKinnell LA (2005) On the global short-term forecasting of the ionospheric critical frequency foF2 up to5 h in advance using neural networks. Radio Sci. https://doi.org/10.1029/2004RS003239

Perna L, Pezzopane M, Pietrella M, Zolesi B, Cander LR (2017) An updating of the SIRM model. Adv Space Res 60(6):1249–1260. https://doi.org/10.1016/j.asr.2017.06.029

Pezzopane M, Scotto C (2005) The INGV software for the automatic scaling of foF2 and MUF(3000)F2 from ionograms: a performance comparison with ARTIST 4.01 from Rome data. J Atmos Solar Terr Phys 67(12):1063–1073. https://doi.org/10.1016/j.jastp.2005.02.022

Pezzopane M, Scotto C (2007) The automatic scaling of critical frequency foF2 and MUF(3000)F2: a comparison between Autoscala and ARTIST 4.5 on Rome data. Radio Sci. 42. https://doi.org/10.1029/2006RS003581

Pezzopane M, Scotto C, Tomasik Ł, Krasheninnikov I (2009) Autoscala: an aid for different ionosondes. Acta Geophys 58(3):513–526. https://doi.org/10.2478/s11600-009-0038-1

Pezzopane M, Pietrella M, Pignatelli A, Zolesi B, Cander LR (2011) Assimilation of autoscaled data and regional and local ionospheric models as input sources for real-time 3-D international reference ionosphere modeling. Radio Sci 46:5009. https://doi.org/10.1029/2011RS004697

Pezzopane M, Pietrella M, Pignatelli A, Zolesi B, Cander LR (2013) Testing the three-dimensional IRI-SIRMUP-P mapping of the iono-sphere for disturbed periods. Adv Space Res 52(10):1726–1736. https://doi.org/10.1016/j.asr.2012.11.028

Pietrella M (2012) A short-term ionospheric forecasting empirical regional model (IFERM) to predict the critical frequency of the F2 layer during moderate, disturbed, and very disturbed geomagnetic conditions over the European area. Ann Geophys 30:343–355. https://doi.org/10.5194/angeo-30-343-2012

Pietrella M (2015) A software package generating long term and near real time predictions of the critical frequencies of the F2 Layer over Europe and its applications. Int J Geosci 6(4):373–387. https://doi.org/10.4236/ijg.2015.64029

Pietrella M, Perrone L (2005) Instantaneous space weighted ionospheric regional model for instantaneous mapping of the critical frequency of the F2 layer in the European region. Radio Sci. https://doi.org/10.1029/2003RS003008

Pietrella M, Pezzopane M (2020) Maximum usable frequency and skip distance maps over Italy. Adv Space Res 66:243–258. https://doi.org/10.1016/j.asr.2020.03.040

Pietrella M, Pezzopane M, Settimi A (2016) Ionospheric response under the influence of the solar eclipse occurred on 20 March 2015: importance of autoscaled data and their assimilation for obtaining a reliable modeling of the ionosphere. J Atmos Solar Terr Phys 146:49–57. https://doi.org/10.1016/j.jastp.2016.05.006

Pietrella M, Pignalberi A, Pezzopane M, Pignatelli A, Azzarone A, Rizzi R (2018) A comparative study of ionospheric IRIEup and ISP assimilative models during some intense and severe geomagnetic storms. Adv Space Res 61(10):2569–2584. https://doi.org/10.1016/j.asr.2018.02.026

Pignalberi A, Pezzopane M, Rizzi R, Galkin I (2018a) Effective solar indices for ionospheric modeling: a review and a proposal for a real-time regional IRI. Surv Geophys 39:125. https://doi.org/10.1007/s10712-017-9438-y

Pignalberi A, Pezzopane M, Rizzi R, Galkin I (2018b) Correction to: effective solar indices for ionospheric modeling: a review and a proposal for a real-time regional IRI. Surv Geophys 39:169. https://doi.org/10.1007/s10712-017-9453-z

Radicella SM, Leitinger R (2001) The evolution of the DGR approach to model electron density profiles. Adv Space Res 27(1):35–40. https://doi.org/10.1016/S0273-1177(00)00138-1

Reinisch BW, Huang X (1983) Automatic calculation of electron density profiles from digital ionograms: 3. Processing of bottom side ionograms. Radio Sci 18(3):477–492. https://doi.org/10.1029/RS018i003p00477

Reinisch BW, Huang X, Sales GS (1993) Regional ionospheric mapping. Adv Space Res 13(3):45–48. https://doi.org/10.1016/0273-1177(93)90246-8

Reinisch BW, Huang X, Galkin IA, Paznukhov V, Kozlov A (2005) Recent advances in real-time analysis of ionograms and ionospheric drift measurements with digisondes. J Atmos Solar Terr Phys 67(12):1054–1062. https://doi.org/10.1016/j.jastp.2005.01.009

Scotto C (2009) Electron density profile calculation technique for autoscala ionogram analysis. Adv Space Res 44:756–766. https://doi.org/10.1016/j.asr.2009.04.037

Scotto C, Pezzopane M (2002) A software for automatic scaling of foF2 and MUF(3000)F2 from ionograms. In: Proceedings of the XXVII general assembly of the international union of radio science, 17–24 August, Maastricht, The Netherlands. International Union of Radio Science, Ghent, CD-ROM

Settimi A, Pezzopane M, Pietrella M, Bianchi C, Scotto C, Zuccheretti E, Makris J (2013) Testing the IONORT-ISP system: a comparison between synthesized and measured oblique ionograms. Radio Sci 48(2):167–179. https://doi.org/10.1002/rds.20018

Settimi A, Pietrella M, Pezzopane M, Bianchi C (2015) The IONORT-ISP-WC system: inclusion of an electron collision frequency model for the D-layer. Adv Space Res 55(8):2114–2123. https://doi.org/10.1016/j.asr.2014.07.040

Singer W, Dvinskikh NI (1991) Comparison of empirical models of ionospheric characteristics developed by means of different mapping methods. Adv Space Res 11(10):3–6. https://doi.org/10.1016/0273-1177(91)90311-7

Stanislawska I, Zbyszynski Z (2002) Forecasting of ionospheric characteristics during quiet and disturbed conditions. Ann Geophys 45(1):169–175

Stankov SM, Jodogne JC, Kutiev I, Stegen K, Warnant R (2012) Evaluation of automatic ionogram scaling for use in real-time ionospheric density profile specification: dourbes DGS-256/ARTIST-4 performance. Ann Geophys 55(2):283–291. https://doi.org/10.4401/ag-4976

Strangeways HJ, Kutiev I, Cander LR, Kouris S, Gherm V, Marin D, De La Morena BA, Pryse SE, Perrone L, Pietrella M, Stankov S, Tomasik L, Tulunay E, Tulunay Y, Zernov N, Zolesi B (2009) Near-earth space plasma modelling and forecasting. Ann Geophys 52(3/4):255–271

Themens DR, Jayachandran PT, Galkin I, Hall C (2017) The Empirical Canadian high arctic ionospheric model (E-CHAIM): NmF2 and hmF2. J Geophys Res Space Phys 122(8):9015–9031. https://doi.org/10.1002/2017JA024398

Themens DR, Jayachandran PT, Bilitza D, Erickson PJ, Häggström I, Lyashenko MV, Reid B, Varney RH, Pustovalova L (2018) Topside electron density representations for middle and high latitudes: a topside parameterization for E-CHAIM based on the NeQuick. J Geophys Res Space Phys 123(2):1603–1617. https://doi.org/10.1002/2017JA024817

Themens DR, Jayachandran PT, McCaffrey AM, Reid B, Varney RH (2019) A bottomside parameterization for the empirical Canadian High Artic Ionospheric Model (E-CHAIM). Radio Sci 54(5):397–414. https://doi.org/10.1029/2018RS006748

Tsagouri I, Zolesi B, Belehaki A, Cander LR (2005) Evaluation of the performance of the real-time updated simplified ionospheric regional model for the European area. J Atmos Sol Terr Phys 67(12):1137–1146. https://doi.org/10.1016/j.jastp.2005.01.012

Tsagouri I, Belehaki A, Bergeot N, Cid C, Delouille V, Egorova T, Jakowski N, Kutiev I, Mikhailov A, Nunez M, Pietrella M, Potapov A, Qahwaji R, Tulunay Y, Velinov P, Viljanen A (2013) Progress in space weather modeling in an operational environment. J Space Weather Space Clim 3:A17. https://doi.org/10.1051/swsc/2013037

Zolesi B, LjR Cander (2014) Ionospheric prediction and forecasting. Springer, Heidelberg. https://doi.org/10.1007/978-3-642-38430-1

Zolesi B, Cander LR, De Franceschi G (1993) Simplified ionospheric regional model for telecommunication applications. Radio Sci 28(4):603–612. https://doi.org/10.1029/93RS00276

Zolesi B, LjR Cander, De Franceschi G (1994) A simple algorithm for regional mid-latitude ionospheric modeling. Adv Space Res 14(12):57–60

Zolesi B, Cander LR, De Franceschi G (1996) On the potential applicability of the simplified ionospheric regional model to different midlatitude areas. Radio Sci 31(3):547–552

Zolesi B, Belehaki A, Tsagouri I, Cander LR (2004) Real-time updating of the simplified ionospheric regional model for operational applications. Radio Sci 39:RS2011. https://doi.org/10.1029/2003RS002936

Zuccheretti E, Tutone G, Sciacca U, Bianchi C, Arokiasamy BJ (2003) The new AIS-INGV digital ionosonde. Ann Geophys IT 46(4):647–659. https://doi.org/10.4401/ag-4377